A COMPLEMENTARY SLOT-DIPOLE ANTENNA
FOR HEMISPHERICAL COVERAGE

BY

W.F. GABRIEL
L. R. DOD

OCTOBER 1966

—— GODDARD SPACE FLIGHT CENTER ——
GREENBELT, MARYLAND

A COMPLEMENTARY SLOT-DIPOLE ANTENNA
FOR HEMISPHERICAL COVERAGE

by

W. F. Gabriel and L. R. Dod

October, 1966

Advanced Development Division
NASA-Goddard Space Flight Center
Greenbelt, Maryland

A COMPLEMENTARY SLOT-DIPOLE ANTENNA
FOR HEMISPHERICAL COVERAGE

by

W. F. Gabriel and L. R. Dod

SUMMARY

A circularly polarized, complementary slot-dipole antenna with hemispherical coverage has been developed for use in a passive interferometer beacon acquisition system. The antenna element consists of a crossed-slot flush mounted in the ground plane, plus a crossed dipole mounted about $0.58\,\lambda$ above the crossed-slot with axes aligned. The crossed-slot is fed from below by means of a circularly polarized waveguide, and the crossed-dipole is fed from a balanced four-wire transmission line which is electrically connected in shunt across the slots. Approximately equal radiated power division is achieved between the crossed-slots and the crossed dipoles which, together with the complementary pattern characteristics of the slot and the dipole, results in a good circular polarization characteristic over most of the hemisphere and permits a reasonably effective approximation to a cosecant-squared power pattern characteristic coverage in elevation except near the horizon. Final design and performance data on the antenna are included.

During the development of this antenna element, several other elevation pattern shaping techniques were investigated and are discussed in the report. These include surface-wave devices, ground plane chokes, and vertical arrays.

CONTENTS

LIST OF FIGURES

LIST OF FIGURES (Continued)

A COMPLEMENTARY SLOT-DIPOLE ANTENNA
FOR HEMISPHERICAL COVERAGE

I. INTRODUCTION

The Apollo Re-Entry Tracking Interferometer is a passive beacon acquisition system. A beacon on the re-entry vehicle radiates an r.f. signal which is received by the interferometer antenna system on earth. The received signal is electronically processed so that the direction angles of the moving vehicle are continuously determined for tracking the vehicle. The mission requirements are explained in reference (1) and the complete electronic system of the interferometer is described in reference (2). This report will be concerned with the interferometer antenna design necessary to meet the mission requirements. The complete system consisting of the interferometer antennas mounted on a groundplane above the equipment van is shown in Figure 1.
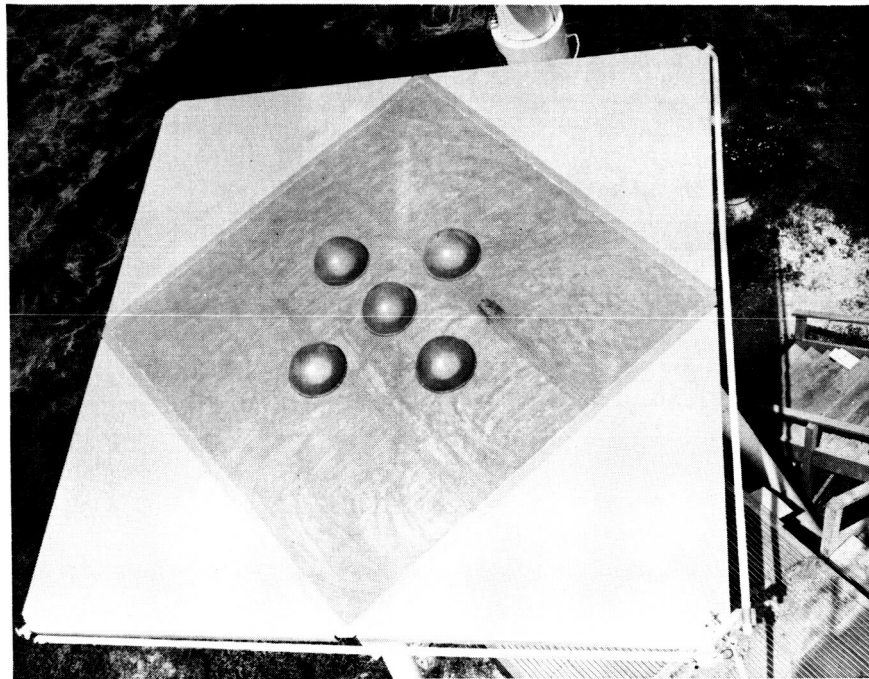
Figure 1—View of Interferometer Antennas and Equipment Van

1

A. Interferometer Principles of Operation

The interferometer is a precise instrument for the measurement of the angular position of a radio frequency source. The interferometer principle is based upon electrical phase difference measurement between two spaced antennas as a function of the physical geometry. Consider two antennas separated by a baseline distance (d) in Figure 2. The wavefront radiated from an r.f. source at point (P) will arrive at antenna (A) first. The path delay before the wavefront reaches antenna (B) is then
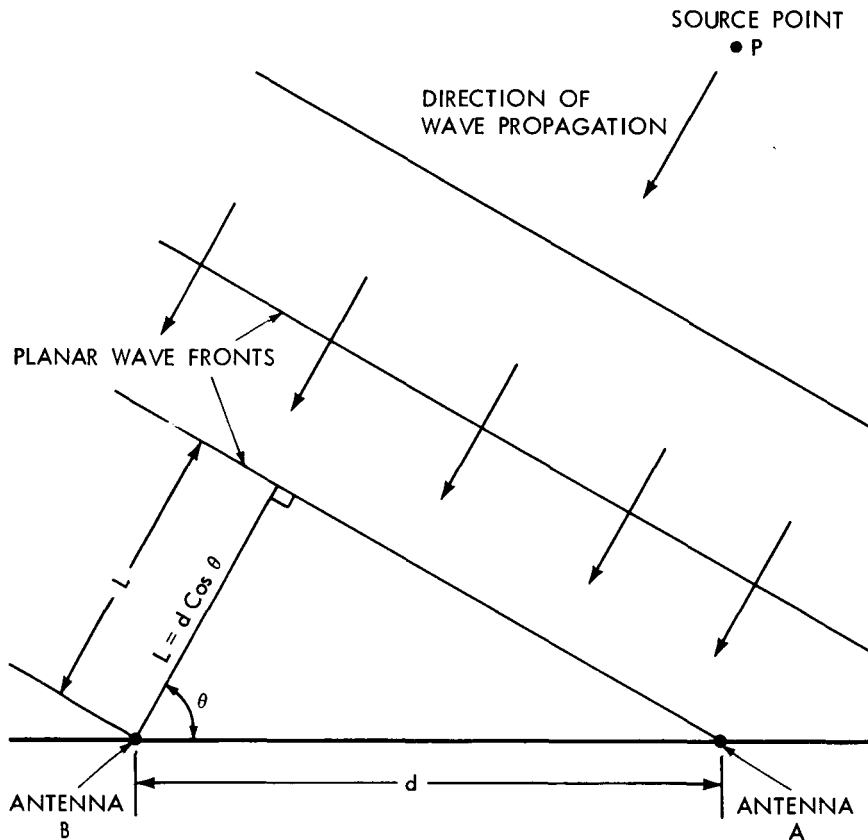
Figure 2—Diagram of Two Antenna Interferometer Showing Electrical Phase Angle Versus Angle of Arrival of Wavefront

$$L = d \cos \theta \tag{1}$$

provided that the source (P) is located a distance from the antennas much greater than the baseline separation (d). The phase delay of the wavefront is then

2

$$\psi = 2\pi \left(\frac{L}{\lambda}\right) = \frac{2\pi d}{\lambda} \cos \theta \text{ Radians} \qquad (2)$$

where λ is the wavelength of the r.f. source at (P). The direction angle of the source, θ, is determined from the measurement of the phase angle, ψ. The actual measuring technique for phase angle is covered in reference (2) and will not be discussed here. Ambiguities do occur in the determination of the angle, θ, since the phase measurement system cannot distinguish between (ψ) and ($\psi + 2\pi n$) Radians where n = 1, 2, 3, ... If the antenna baseline (d) exceeds $\lambda/2$, the interferometer has multiple space angles, θ, for the same measured value of ($\psi + 2\pi n$). However, the sensitivity of the interferometer increases with the baseline length, d, since the phase change per space angle

$$\frac{d\psi}{d\theta} = \frac{2\pi d}{\lambda} \sin \theta \qquad (3)$$

is directly proportional to the magnitude of d. The rate of change of phase angle with space angle is maximum for $\theta = 90°$ and minimum for $\theta = 0°$. Thus, the interferometer has its greatest sensitivity normal to the baseline and least sensitivity along the baseline. The interferometer technique can be extended to three dimensions by the addition of a second baseline at right angles to the baseline just described. Figure 3 shows the crossed baselines with space angles θ and φ used to describe the point P.

Ambiguities in the space angle θ are resolved by the following method. Multiple interferometers are formed by three colinear antennas with the spacings shown in Figure 4. The method used for resolving the ambiguities is to simultaneously measure the phase between antenna pairs 1-3 and 1-2. The difference in phase between the two pairs of antennas is then subtracted electronically. If this calculated difference is now subtracted from the phase measurement for antenna pair 1-2, the resultant is equivalent to the phase measurement between a pair of antennas with $\lambda/2$ spacing. As mentioned previously, a spacing of $\lambda/2$ has no ambiguities in the angle θ so that the angle is resolved.
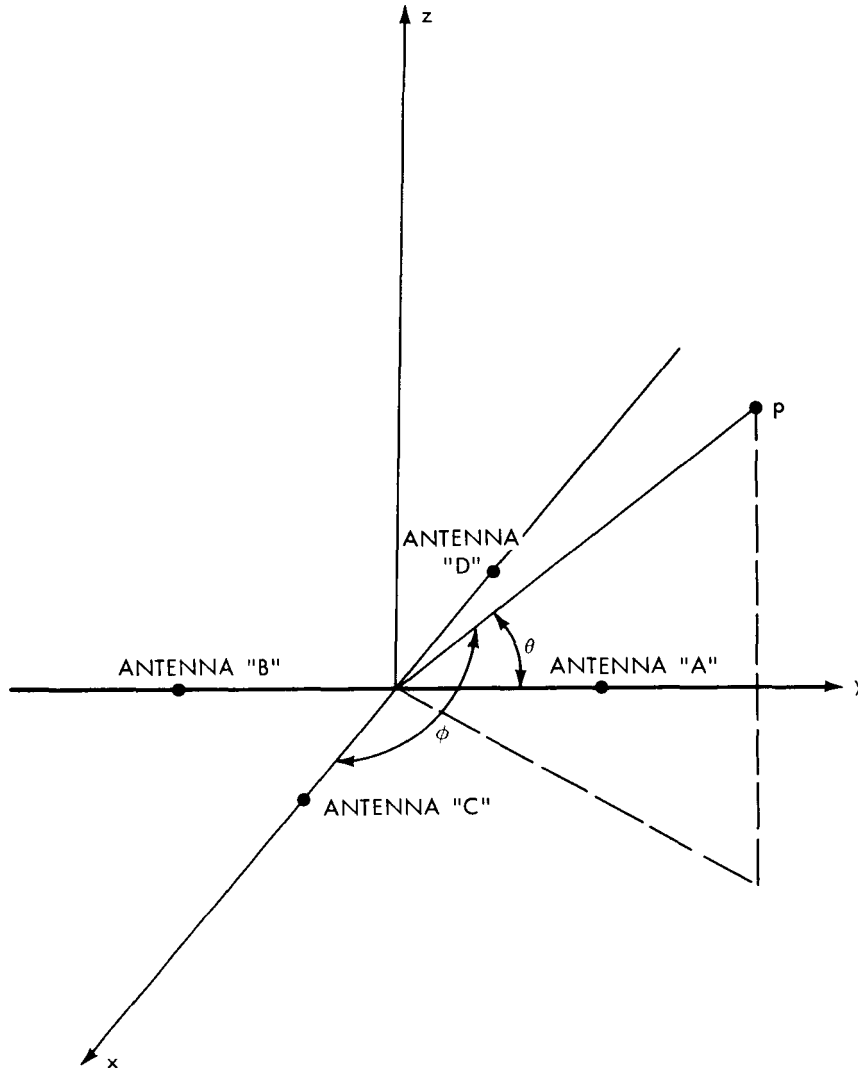
Figure 3—Diagram of Crossed Baseline Interferometers With Angles
θ and ϕ to Describe the Field Point (P)

B. Antenna Requirements

The crossed horizontal baselines of the Re-Entry Tracking Interferometer
are shown in Figure 5. Antenna pairs 1-3 and 4-5 form two orthogonal 10.5 λ
baselines. Antenna 2 is common to both baselines and is used to resolve ambi-
guities in the direction angles of the source. Each antenna must be circularly
polarized to insure maximum reception time from the linearly polarized beacon
antenna, regardless of spacecraft orientation. The uncertainty of the re-entry
trajectory requires that the interferometer have a nearly hemispherical cover-
age as discussed in reference (1). It is desirable to have a response pattern that

4

covers 360° in azimuth and all elevation angles greater than 10° above the horizon. The response pattern desired in the vertical plane is similar to the response of a ground-based aircraft search radar. The response pattern frequently approximated in search radars is

$$E = Csc \; \theta = \frac{r}{h} \tag{4}$$

where E is the received signal level, θ is the elevation angle, r is the slant range, and h is the height of the vehicle (reference 3). If the re-entry vehicle is at a constant height, the received signal will be proportional to the range, r.
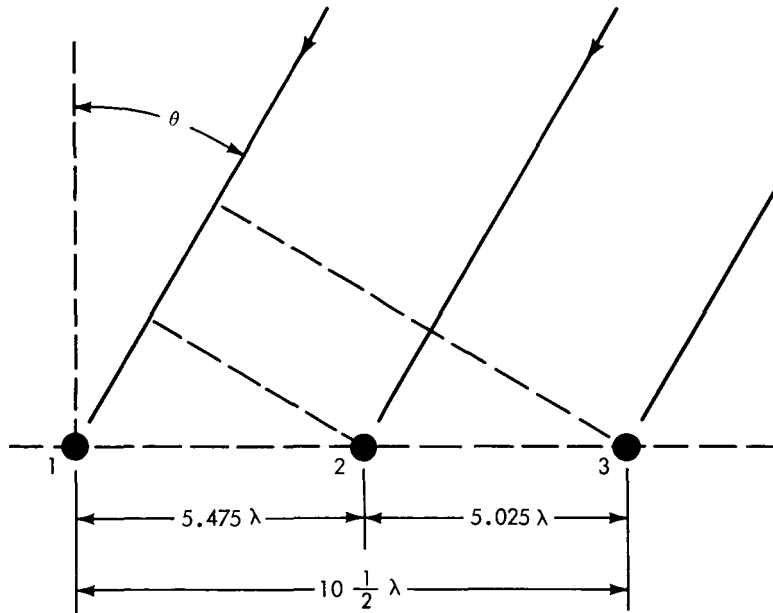
PHASE $= \phi = \dfrac{2 \pi d}{\lambda} \sin \; \theta$

MEASURE $\quad \phi_{13} = 21 \pi \sin \theta =$ fine resolution

MEASURE $\quad \phi_{12} = 10.95 \pi \sin \theta$

$\phi_{23} = \phi_{13} - \phi_{12} = 10.05 \pi \sin \theta$

$\phi_{12} - \phi_{23} = 0.90 \pi \sin \theta =$ coarse resolution

(equivalent to $< \dfrac{\lambda}{2}$ spacing)

Figure 4—Diagram of Antennas With Ambiguity Resolving
Equations Included

5
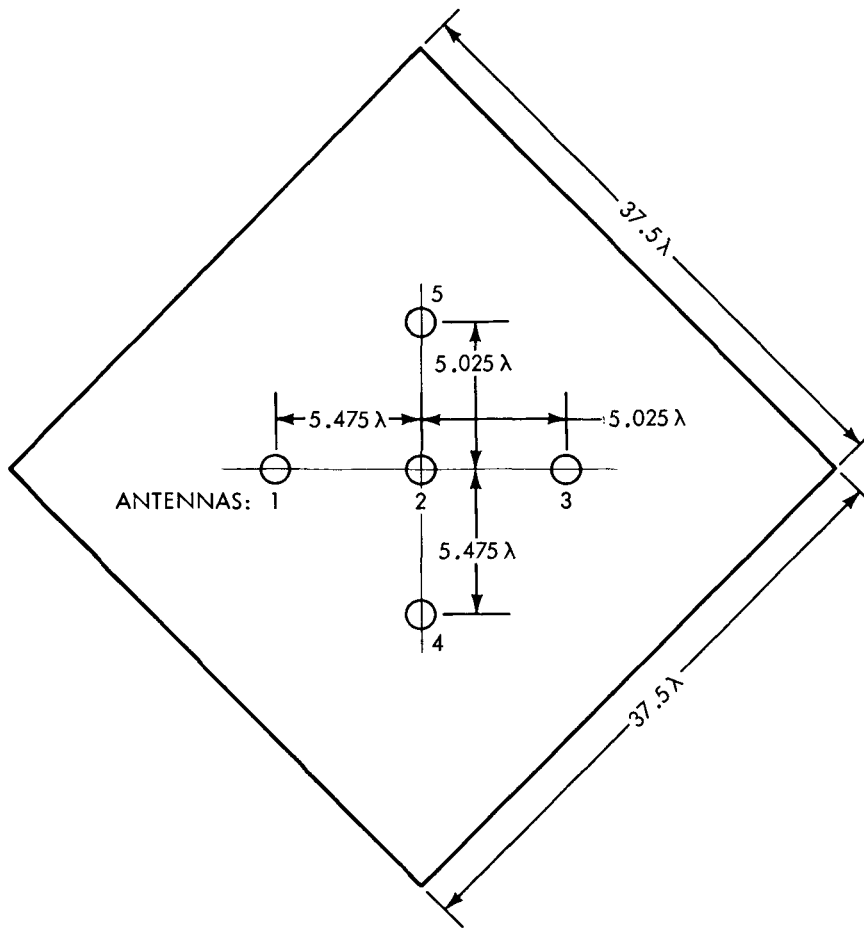
Figure 5—Diagram Showing Interferometer Antenna Separation
(Crossed Baseline)

The methods for achieving the cosecant response pattern by the design of the individual antennas is discussed in section II.

The bandwidth of the system is defined by the maximum Doppler shift of the r.f. signal caused by the motion of the vehicle since the tracking beacon signal is a pure carrier with no modulation (reference 4). For a vehicle speed of 7.5 km/sec (reference 1), the maximum possible Doppler shift is ±57.3 KHz. from the signal frequency of 2287.5 MHz.

Since the final installation of the interferometer is on a tracking ship, the groundplane containing the interferometer antennas is limited in size. A finite groundplane will cause the interferometer antennas to have a response at angles below the horizon due to diffraction effects at the groundplane edges. Such a response, which is generally referred to as "back-radiation," will cause phase

measurement error because of reflections from the sea surface. If a direct ray and a sea-reflected specular ray are added vectorially, the phase error can be calculated. The largest phase error will occur when the two signals are in quadrature. For the error limit of 0.1 degree which has been established for the system (reference 2), the quadrature reflected signal would have to be -53 db with respect to the direct ray. Since the reflected rays from the sea surface are randomly phased, the requirement on back-radiation level need not be as severe as -53 db. However, it is considered desirable to keep the back-radiation level below -30 db in order to hold down this source of error.

The accuracy required in laying out the baselines may be obtained from the phase equation (2). The phase angle error, $\delta\psi$, due to an error in baseline length, δd, is derived in Appendix I and found to be

$$\delta\psi = \frac{2\pi \delta d}{\lambda} \cos \theta \qquad (5)$$

where θ is the angle from the baseline. For an elevation angle, θ, of 10 degrees, and a baseline measurement tolerance, δd, of 0.003 inches, the phase error is 0.172 degrees. This error will decrease as the elevation angle, θ, is increased since $\delta\psi \approx \cos \theta$.

II. BASIC ANTENNA TECHNIQUES INVESTIGATED

The task of attempting to satisfy the various antenna requirements formulated in the preceding section was approached by first investigating several basic antenna techniques which were considered applicable. These techniques included:

A. Vertical Arrays of Elements

B. Complementary Slot-dipole Combinations

C. Groundplane Effects

D. Groundplane Choke Devices

E. Groundplane Surface-wave Devices

ZENITH

ϕ

DIPOLE LOCATION

GROUNDPLANE

h

h

DIPOLE IMAGE LOCATION
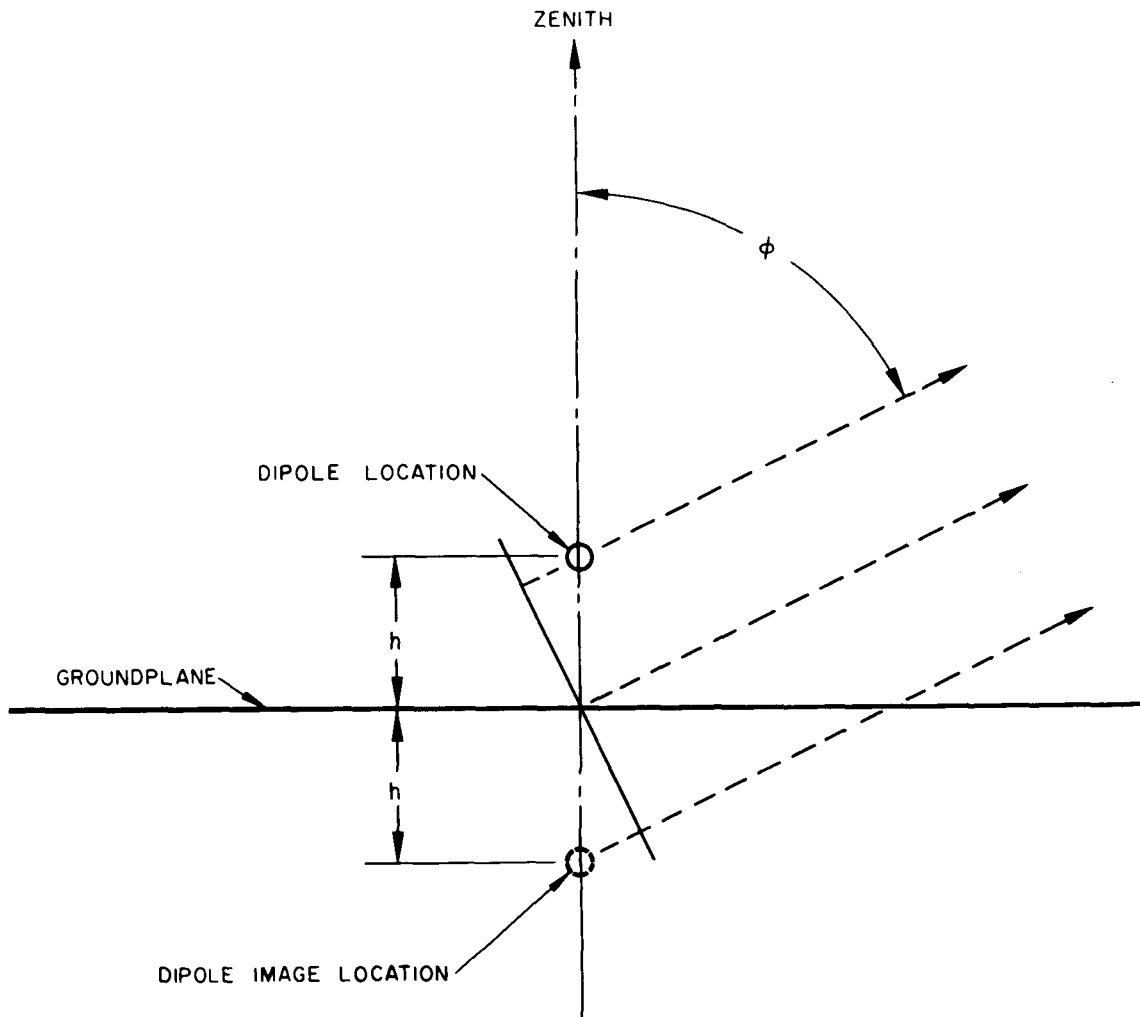
Figure 6—Geometry of Dipole Over Groundplane and Its Image

Other techniques such as resistive groundplanes, horizontal arrays, and dielectric pattern-shaping lenses were also considered, but the nine-month study program did not permit the time that would be required to investigate these additional approaches.

A. Vertical Arrays of Elements

Vertical arrays were the first technique considered for the interferometer antenna because of their natural application in controlling the shape of the vertical-plane pattern. Here, the most simple array possible is a horizontal dipole mounted over a groundplane; i.e., the dipole plus its groundplane image form a two-element vertical array as illustrated in Figure 6. The voltage associated with the dipole image will always be equal in amplitude and opposite in phase to

8

the dipole itself, so that the phase-center will be located on the surface of the groundplane at the point directly beneath the dipole. From the simple geometry of this array as sketched in Figure 6, it is readily shown (5) that the total field, E, at a large distance for the direction φ from zenith may be written as

$$E = A(\varphi) \cdot \sin u \tag{6}$$

where

$$u = \frac{2\pi h}{\lambda} \cos \varphi \tag{7}$$

$A(\varphi)$ = element field intensity amplitude as a function of φ.

h = height of dipole above groundplane.

λ = wavelength.

For a dipole, the element field intensity amplitude patterns in the E-plane and H-plane may be approximated by the expressions, (5)

$$\text{(E-plane)} \quad A_E(\varphi) \approx \cos \varphi \tag{8}$$

$$\text{(H-plane)} \quad A_H(\varphi) = 1 \tag{9}$$

so that the total field intensities in the principal pattern planes become

$$\text{(E-plane)} \quad E_E \approx \cos \varphi \sin u \tag{10}$$

$$\text{(H-plane)} \quad E_H \approx \sin u. \tag{11}$$

9

An examination of the (sin u) function indicates that a pattern approximating the ideal cosecant coverage will be obtained when the dipole is located about 0.45 λ above the ground plane. Also, the extra cos φ factor in the E-plane pattern portends an inherently poor circular polarization ellipticity ratio for φ angles beyond about 45 degrees. These two characteristics are illustrated by Figure 7, which contains actual E-plane and H-plane power patterns measured on a typical dipole mounted 0.45 λ above a 14 λ square groundplane. It will be noted that the H-plane pattern of the dipole comes reasonably close to satisfying the coverage requirement.

By increasing the number of elements above the groundplane to two or more, one can take advantage of the flexibility in amplitude, spacing, and phasing of the elements to obtain better vertical pattern control. For the reader who may be unfamiliar with array pattern synthesis techniques, Jordan (6) provides a particularly simple explanation by making a direct analogy to waveform synthesis with a Fourier series of a given number of terms (elements). The equations for field intensity become quite complicated, of course, and require computer assistance in sifting through the hundreds of amplitude, spacing, and phase combinations that are possible with even a modest array of four or five elements.

The theoretical advantage in vertical pattern control offered by an array of several elements was offset, in this particular case, by a number of other factors which could not be satisfactorily resolved within the allotted time. The principal difficulty was that of developing an element (or a combination of elements) which could be stacked vertically in such a manner as to permit individual feeding adjustments and have good circular polarization performance over the complete hemisphere. The most suitable type of "element" for this application appeared to be the near-isotropic, circularly polarized antenna discussed by Galindo (7) and Green. This particular antenna consists of a ring of crossed slots excited for circular polarization, with the slots progressively phased around the ring so as to form the correct sense of circular polarization in the zenith axial direction as well as in the plane of the ring. The development time estimated for adapting this type of element into a stacked vertical array prototype far exceeded the nine months available, so that the concept was abandoned. Other factors that adversely affect a vertical array of several elements for this particular application include the shadowing effects of one array upon another, mutual coupling effects between arrays, and movement of the array phase center vs. elevation angle caused by the inverted directivity contributions from the groundplane image of the array.

10
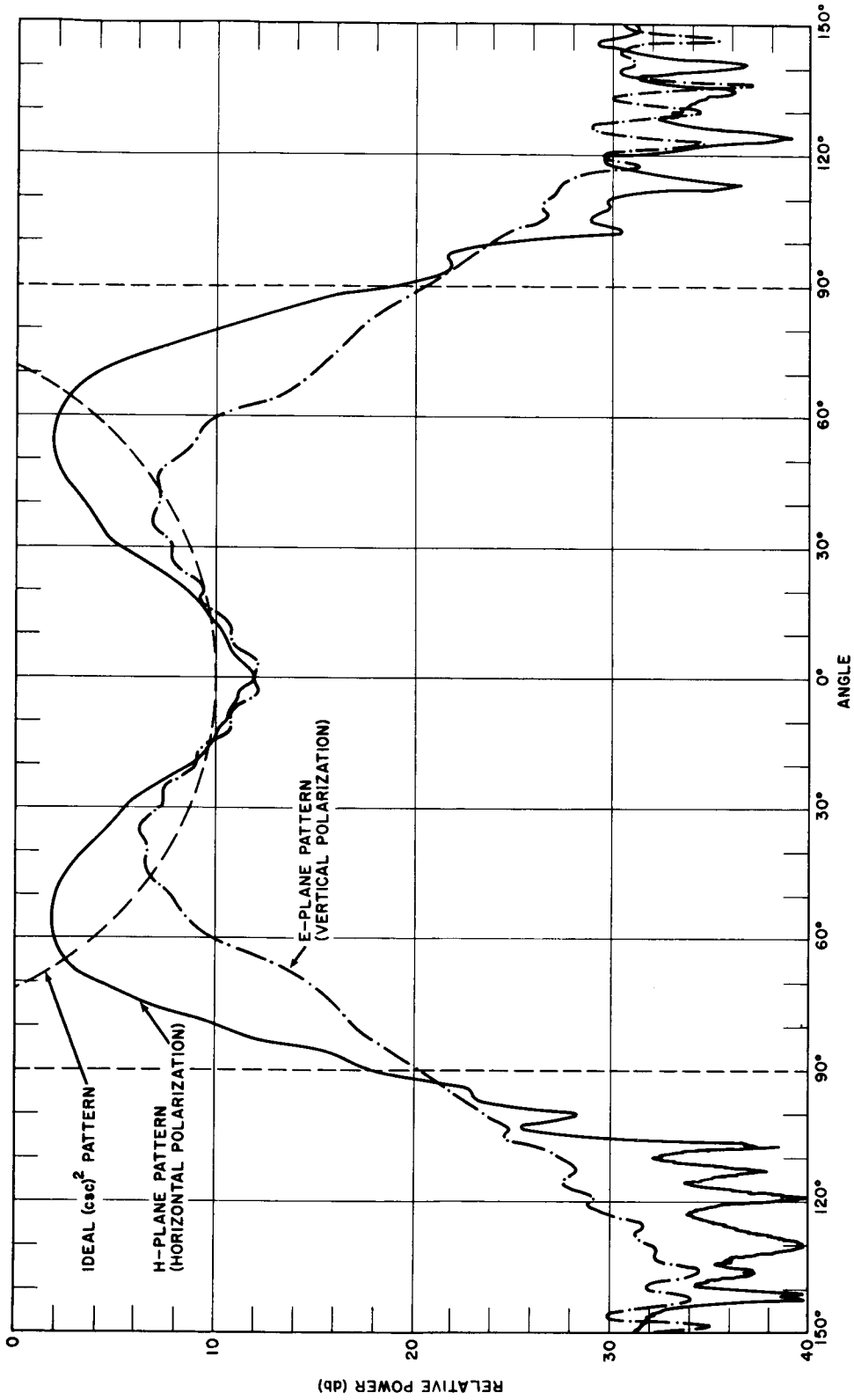
Figure 7—Typical Patterns of a Dipole Mounted 0.45 λ Above a 14 λ Square Groundplane

11

B. Complementary Slot-Dipole Combinations

The dipole pattern characteristics exhibited in Figure 7 led to the conjecture that an improvement in the E-plane coverage could be effected by appropriate combining of a dipole radiator with a complementary slot radiator. Typical pattern characteristics of a slot in a large groundplane are shown in Figure 8.

Several slot-dipole configurations were tried, of which the two most successful are shown in Figure 9. The slot-dipole of Figure 9a consists of a crossed-dipole scatterer mounted on top of a dielectric rod which is, in turn, mounted on top of a crossed-slot on the ground-plane surface. The dipole axes are exactly aligned with the slot axes. A portion of the energy radiating from the slot is coupled into the dipole via the dielectric rod, and the dipole then radiates. This combination can be "tuned" at any given frequency by variation of the dipole dimensions and the dielectric rod dimensions, and a set of typical patterns is shown in Figure 10. It will be noted here that the E-plane and H-plane patterns match up fairly well.

The slot-dipole antenna of figure 9b consists of a crossed, folded dipole fed from a balanced four-wire transmission line which is electrically connected in shunt (via the transmission lines lying over the groundplane) across the flush mounted crossed-slot. This combination is more versatile than the antenna of Figure 9a because of the fact that it is easier to adjust the power division and phase of the dipole radiation relative to the slot radiation via impedance control and line-length phasing. A typical set of patterns is shown in Figure 11, and here it will be noted that the E-plane pattern has been improved considerably over that shown in Figure 7.

The complementary slot-dipole antenna was considered to be a practical solution to the interferometer application such that it was developed further toward a prototype model, as discussed in Section III to follow.

C. Groundplane Effects

A precision interferometer with hemispherical coverage should have the elements mounted on a common groundplane in order to minimize the interfering effects which can arise from the local site environment of the antenna. This groundplane becomes an integral part of each element of the interferometer and, in fact, defines the boundary of an "aperture". from which the element radiates. Figure 12 illustrates the two principal radiation contributions involved at the groundplane "aperture". The main contribution is represented by the hemispherical wavefront emanating from the phase center of the element plus its groundplane image. By applying Huygen's principle, (8), one can readily represent
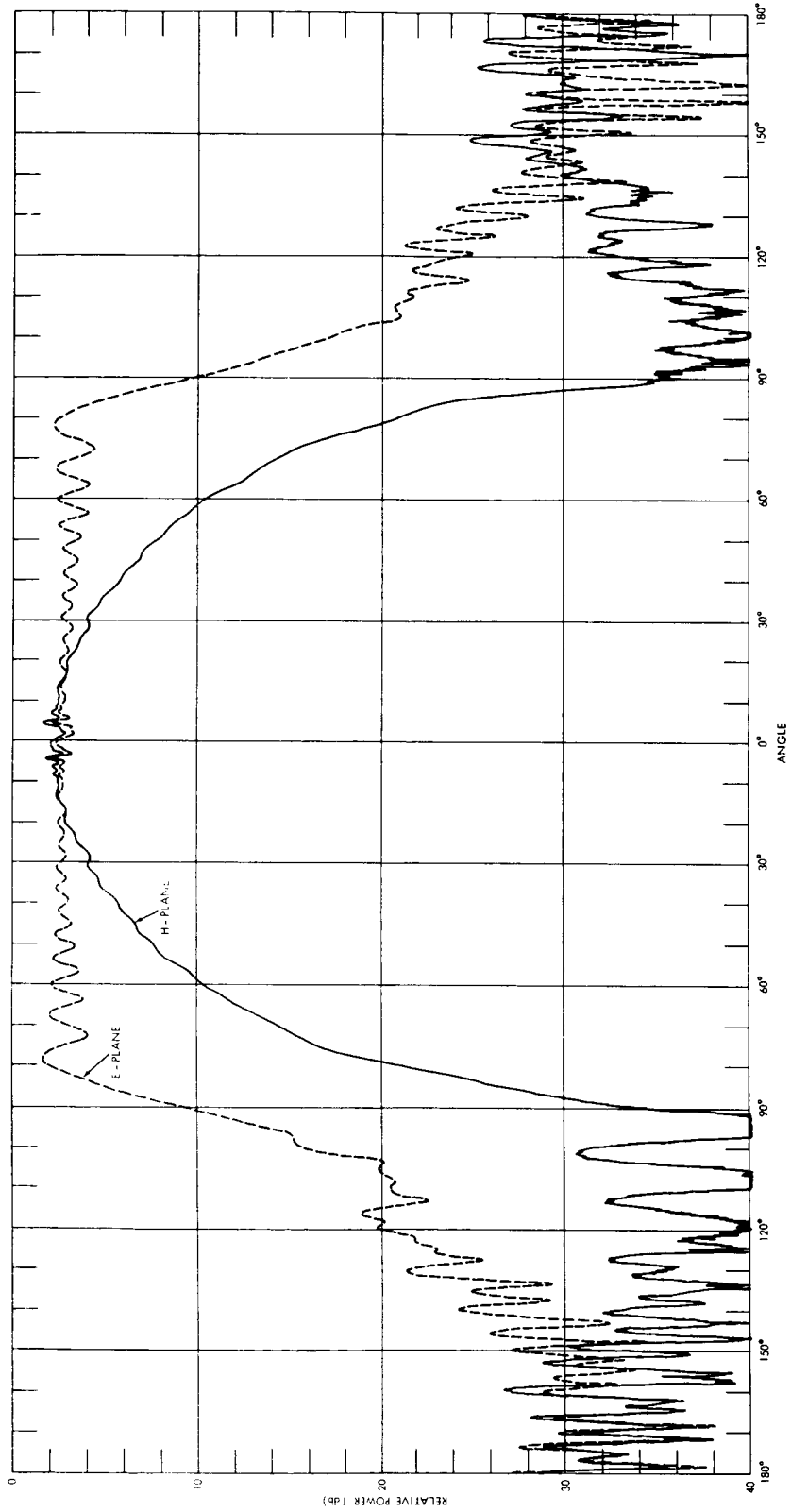
Figure 8—Typical Patterns of a $\lambda/2$ Slot Radiator in a 25 λ Square Groundplane; Diagonal Orientation
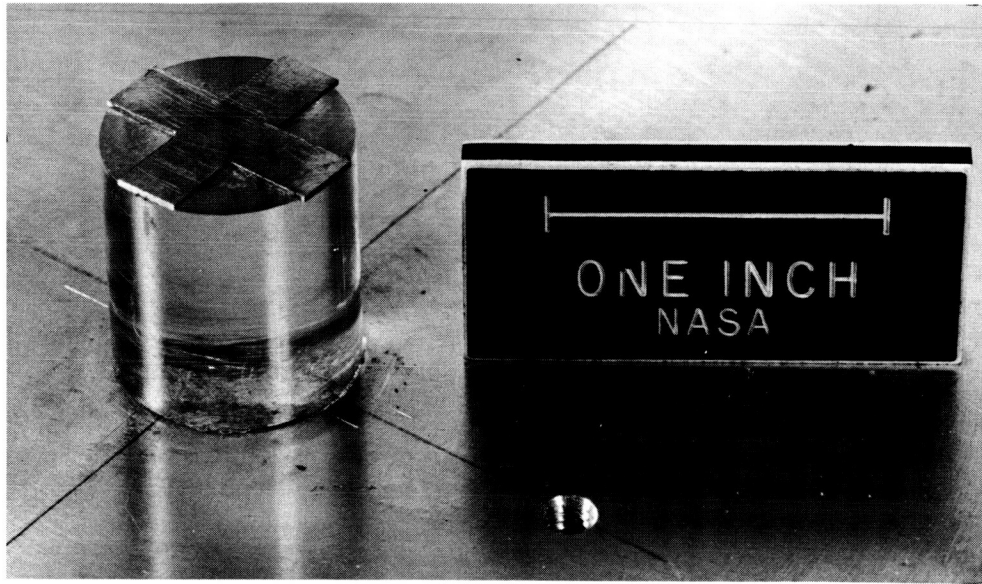
(a) Dipole Scatterer Fed From Dielectric Rod
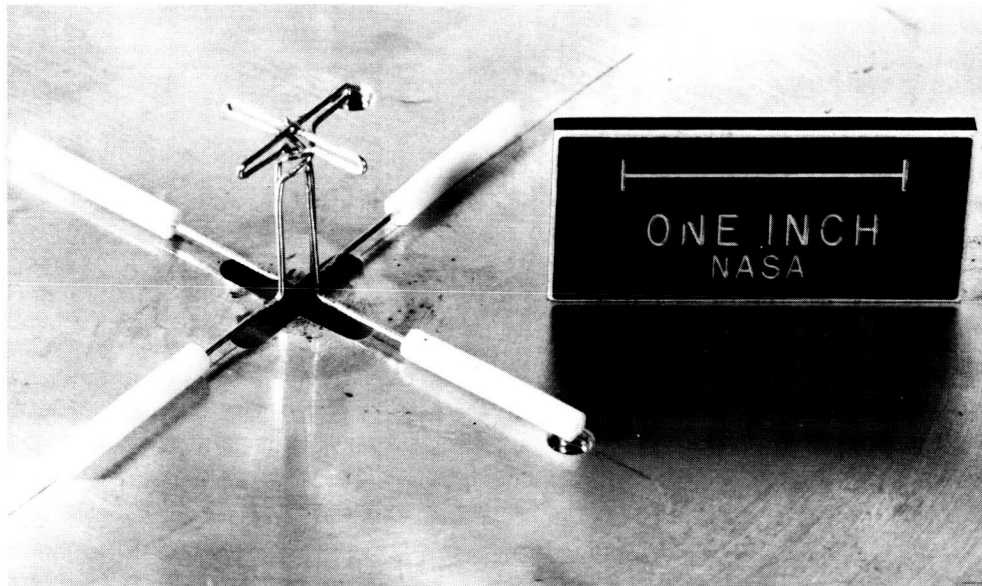
(b) Folded Dipole Fed From Transmission Line

Figure 9—Examples of Complementary Slot-Dipole Antennas Modeled at X-Band.

14
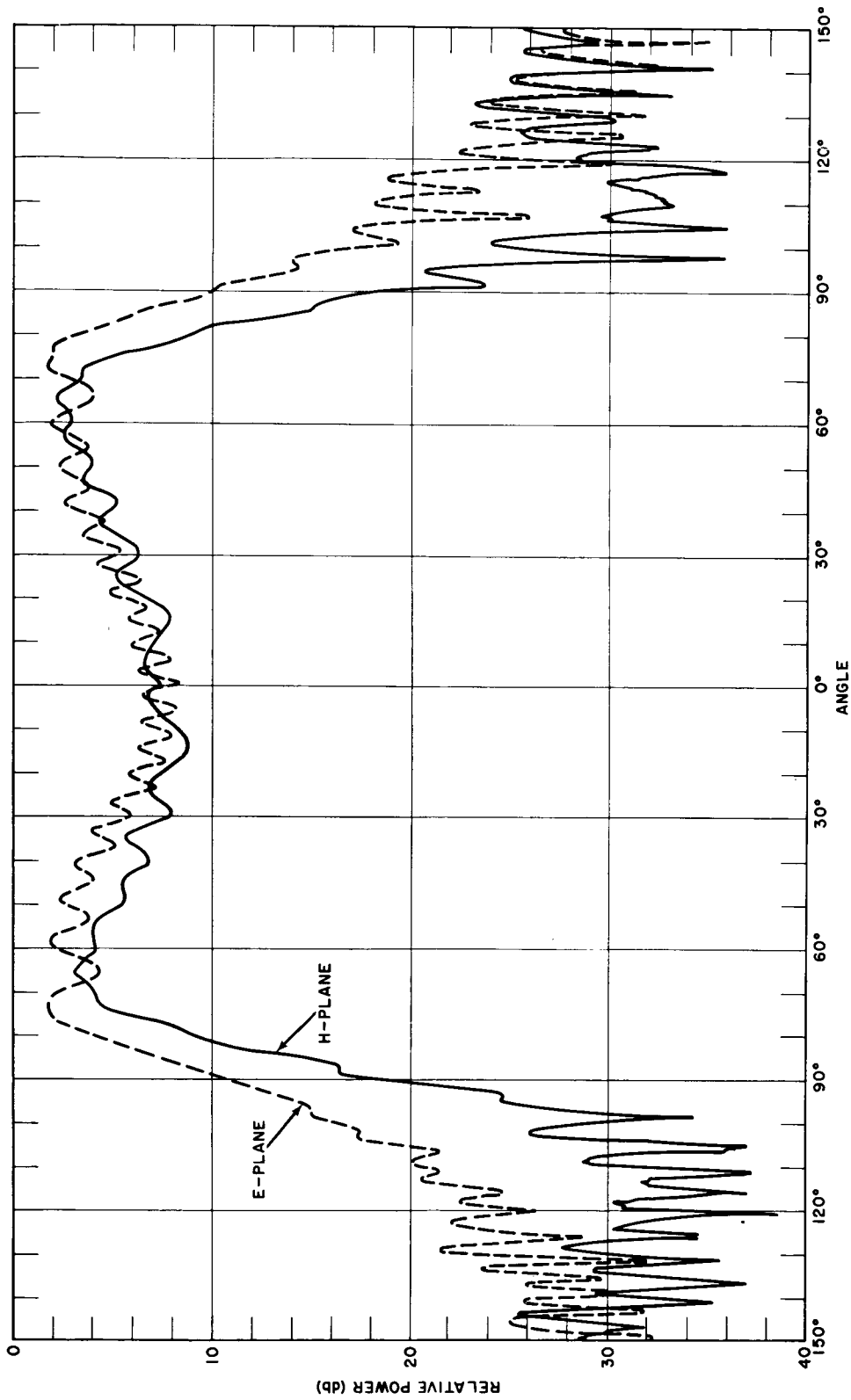
Figure 10—Typical Patterns of Crossed-Dipole Mounted on Dielectric Rod, Slot Fed,
Modeled at X-Band on an 18λ Square Groundplane

15
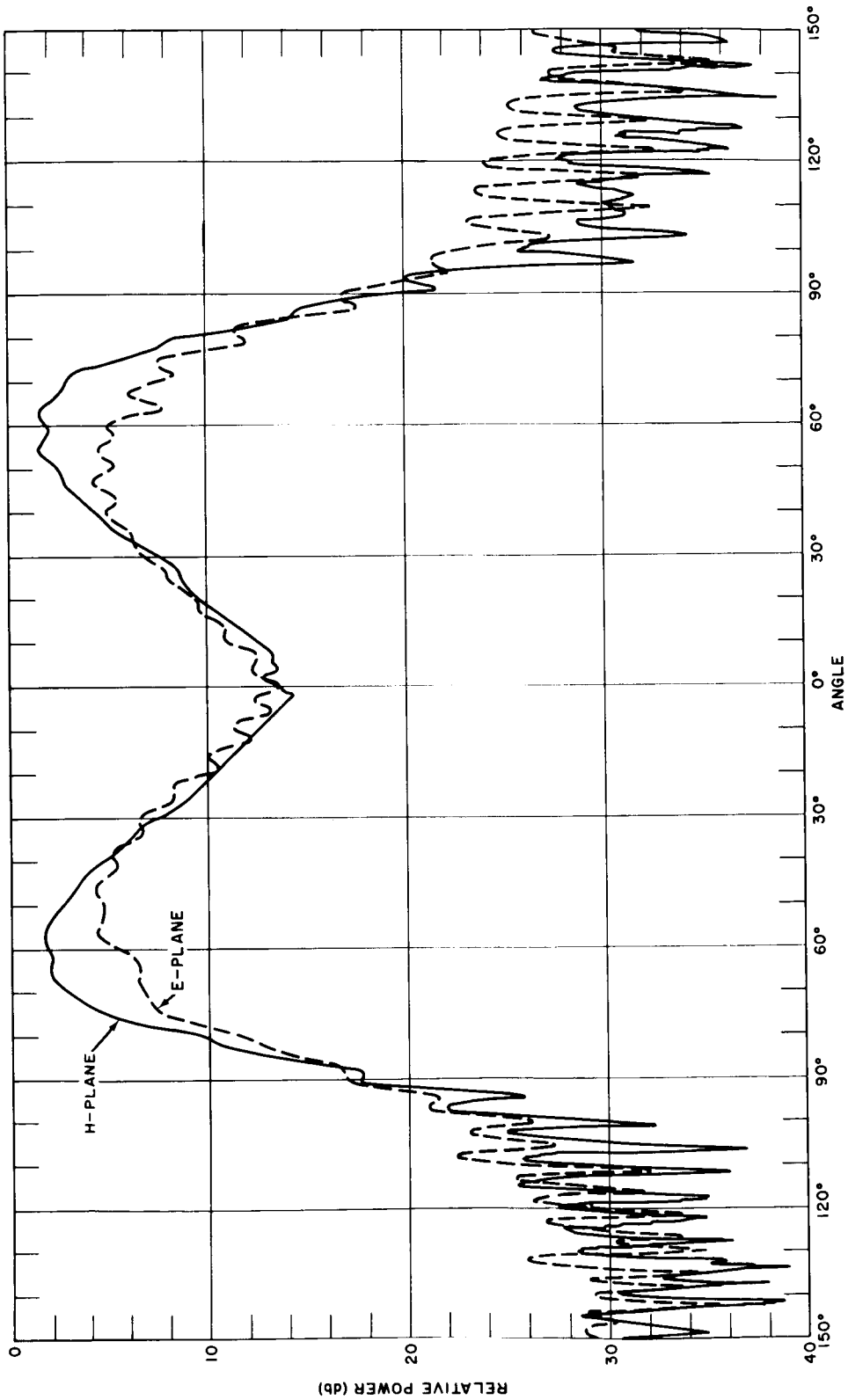
Figure 11—Typical Patterns of a Crossed, Folded Dipole, Transmission-Line Fed From a Radiating Crossed-Slot. Modeled at X-Band on an 18 λ Square Groundplane.

16
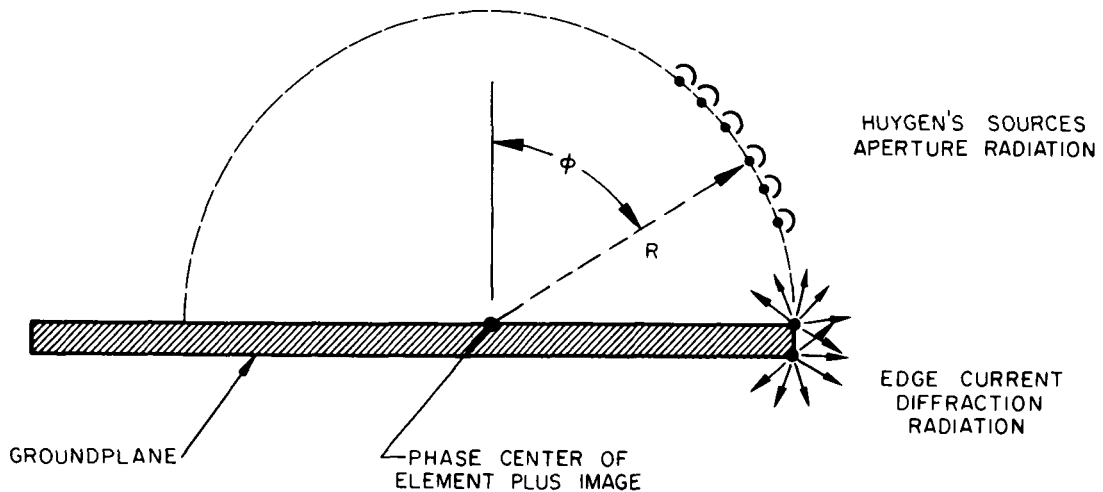
Figure 12—Simple Illustration of Groundplane "Aperture" Radiation Contributions

the radiation from this region with a distribution of equivalent Huygen's sources. It will be recognized that at the edge of the groundplane, the situation is similar to the classical problem of diffraction at a straightedge (8).

The secondary contribution to groundplane effects is the radiation that occurs at the edges of the groundplane due to excitation by radial current field components. Note that an E-field perpendicular to the groundplane will have a radial current associated with it as, for example, in the E-field from a slot radiator. This edge diffraction radiation does not usually affect the upper hemispherical coverage pattern to a significant degree (there are exceptions to this statement), but it always affects the back-radiation and can produce excessively high back-lobes. It is the back-lobe problem that makes radial current excitation of the groundplane edges very undesirable.

Precise analytical treatment of edge diffraction is a very tedious task, and the interested reader is referred to the literature for further discussion of the subject as, for example, in the article by Russo, et al., (9).

D. Groundplane Chokes

Groundplane chokes are sometimes utilized for controlling back-radiation and achieving pattern shaping. Examples of their use include the S-band shaped-beam feed developed at JPL, (10), and the beam-shaping feedhorn described by A. F. Kay (11,12) wherein negative reactance wall surfaces are used.

In the case of a quarter-wave choke groove, its purpose is to present a very high impedance to the radial current flow along the surface of the groundplane, thereby terminating the radial current and forcing abrupt radiation of the power contained in the near-surface fields associated with the current. Figure 13 illustrates a simple geometry for abrupt choke radiation, from which one can write the total field intensity in the direction φ as the vector sum of the element contribution, $\overline{E}_1$, plus the choke radiation, $\overline{E}_2$,

$$\overline{E} = \overline{E}_1 + \overline{E}_2 \tag{12}$$

$$\overline{E} = A_1(\varphi)\, e^{jx\sin\varphi} + A_2(\varphi)\, e^{j(x+\alpha)} \tag{13}$$

where $\quad x = \dfrac{2\pi d}{\lambda}$

α = fixed phase angle for choke radiation relative to element. $\alpha \approx \pi$.

$A_1(\varphi)$ = amplitude of element radiation.

$A_2(\varphi)$ = amplitude of choke radiation.

The phase difference between vectors $\overline{E}_1$ and $\overline{E}_2$ would therefore be

$$\text{phase difference} = \frac{2\pi d}{\lambda}\,(1 - \sin\varphi) + \alpha. \tag{14}$$

A brief inspection of the oscillating behavior possible in the amplitude of $\overline{E}$ versus φ for various values of d points up its application in the JPL feed design where $d \approx 2\lambda$. However, this type of choke radiation pattern shaping could not be applied to the interferometer elements because the oscillations are not compatible with the cosecant pattern shape desired.

The most practical use found for quarter-wave chokes was to install them around the periphery of a large groundplane in order to reduce back-radiation from radial currents which have already been reduced in amplitude via some other technique. Figure 14 illustrates such an application, where a peripheral ring about 2-1/2 λ in width and consisting of 16 quarter-wave choke grooves was installed around a circular groundplane of about 17 λ diameter. The choke
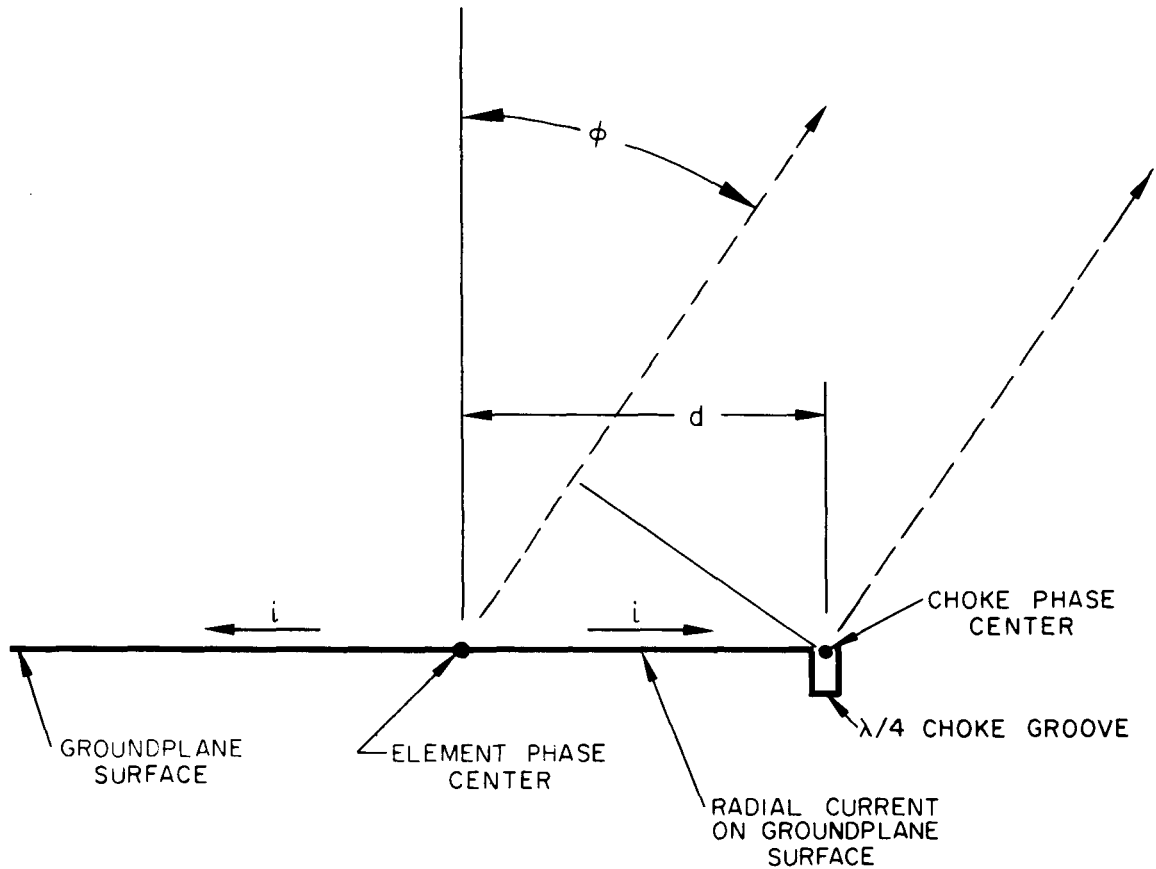
Figure 13—Geometry of Abrupt Choke Radiation

grooves were loaded with absorbing material in this particular instance because the circular symmetry of the abrupt choke radiation with respect to the centered crossed-slot radiator resulted in too much interference with the slot pattern; i.e., the energy associated with the radial current was partly absorbed instead of being entirely radiated. This choke ring dropped the back radiation below the -30 db, level.

The negative reactance surface described by Kay, (11, 12), which calls for a choke groove depth between $\lambda/4$ and $\lambda/2$ in order to be capacitive, was not actually carried to the experimental investigation stage during this study. However, the technique appears to be very attractive as a means for converting the radial current field components into controlled "leaky" radiation such that the fields are essentially lifted off of the groundplane surface and thereby cannot contribute undesirable edge diffraction effects.

Figure 14—Example of a Peripheral Quarter-Wave Choke Ring Installed Around a 17λ Diameter Circular Groundplane Containing a Crossed-Slot Radiator In Combination with a Phased Surface-Wave Launcher. Modeled at X-Band.

E. Groundplane Surface-Wave Devices

Surface-wave devices were investigated because they offered a means for converting the radial current field components into a trapped groundplane surface-wave which could then be launched as a controlled surface-wave radiation. Unlike the negative reactance surface described by Kay, a surface-wave device is a positive reactance surface (13); i.e., it is inductive or "slow wave." An inductive surface is readily designed by utilizing grooves or corrugations (13) with a depth of less than $\lambda/4$ in the groundplane surface, as illustrated by the central region of Figure 14. In order to avoid excessive abrupt radiation, it is necessary to provide a gentle taper in groove depth into the trapped surface-wave region.

After reaching the desired inductive groove depth of approximately $\lambda/8$, the depth is kept constant for a distance which is adjusted so as to result in the surface-wave radiation being exactly 180° out-of-phase with the direct radiation from the crossed-slot at the horizon. The groove depth is then gently tapered back to zero in order to set up a loosely bound surface-wave for launching. A simplified sketch of the geometry is shown in Figure 15, where the distance to the effective phase center of the launched surface-wave is denoted by d. It will

20
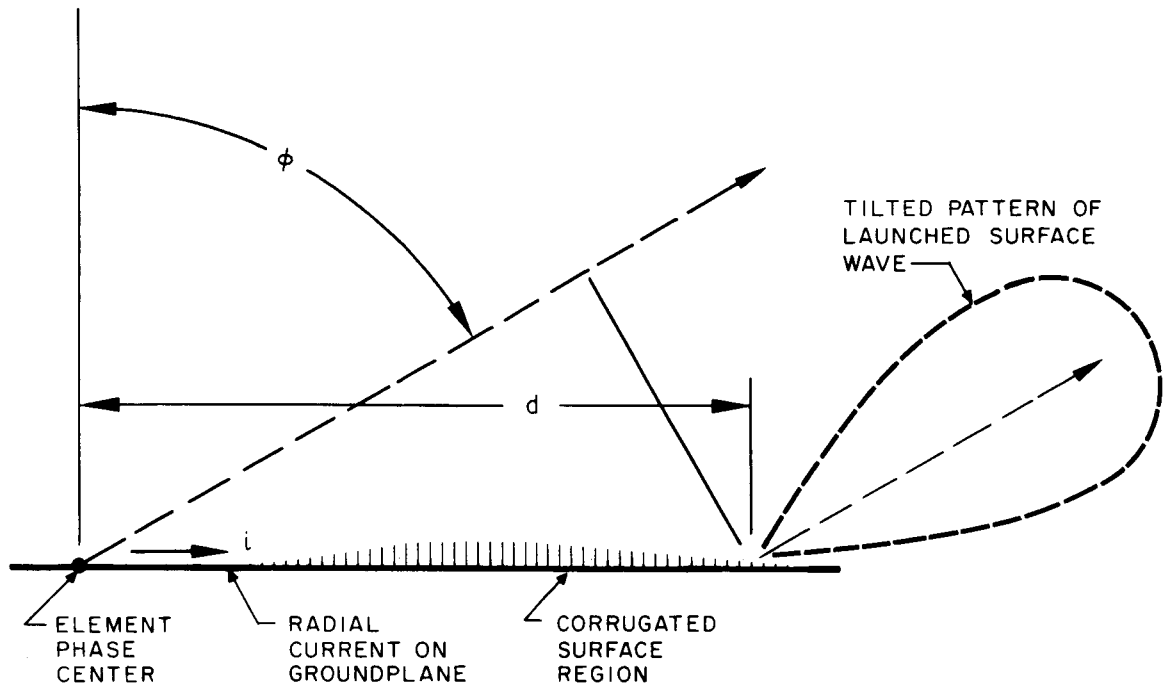
Figure 15—Geometry of Surface Wave Radiation

be noted that the total field intensity can be represented in the same manner as discussed previously for the choke, so that equations (12), (13), and (14) apply equally well here. The launched surface-wave has an amplitude pattern, $A_2(\phi)$, which is tilted up about 20° to 30° above the horizon. (13)

Figure 16 illustrates the improvement in horizon and back-radiation level that can be obtained with one of these tapered surface-wave devices in combination with a crossed-slot. The "rabbit ears" on the surface-wave combination pattern are caused by the tilted pattern amplitude of the surface-wave radiation and are typical of this type of antenna. It will be noted that an improvement of about 14db. can be obtained at the horizon, but only at the expense of some degradation at elevation angles near 10 degrees.

It was concluded that surface-wave devices were not practical for the interferometer application because of the "rabbit ears" pattern characteristic, the
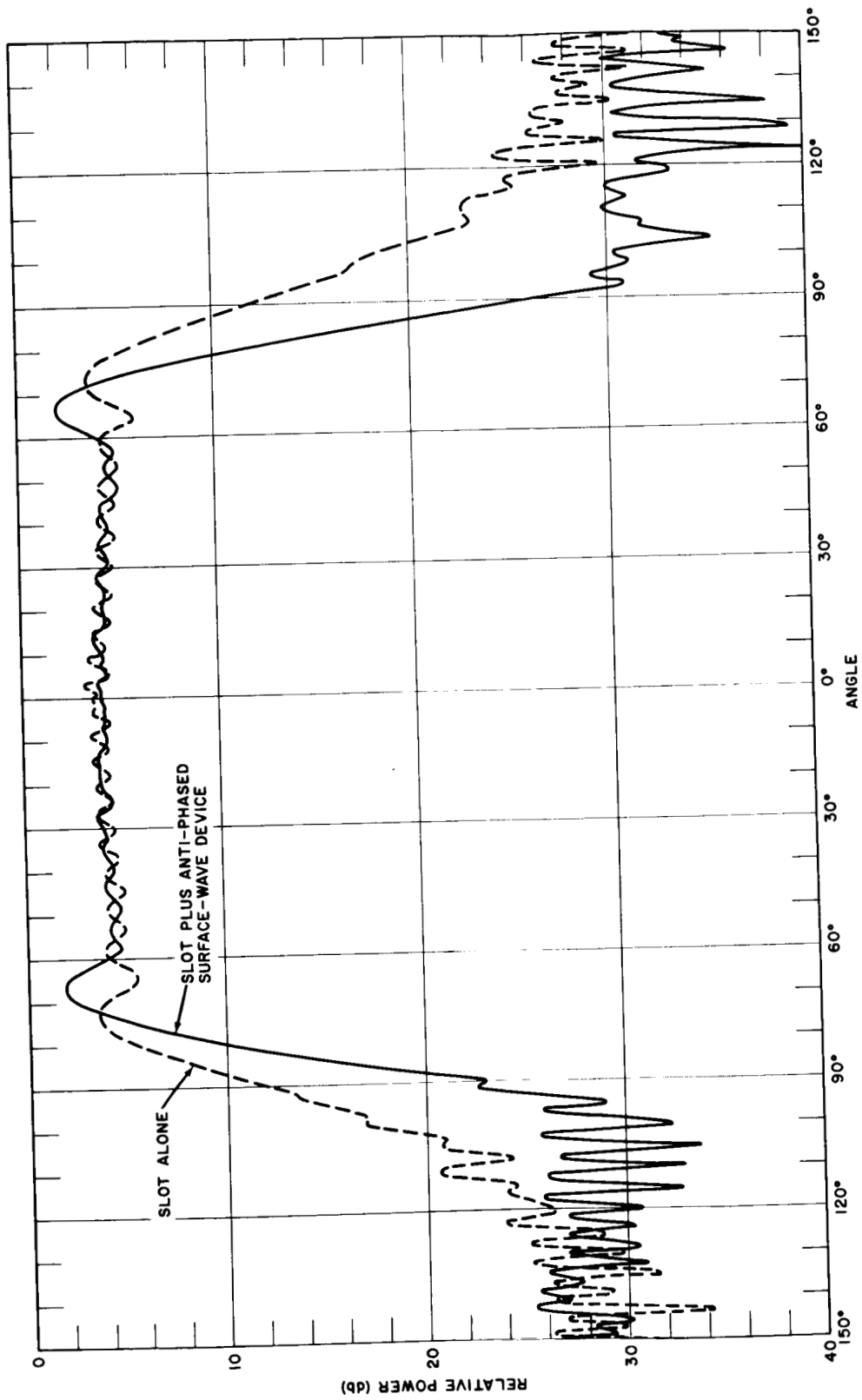
Figure 16.–E-Plane Patterns of a Crossed-Slot in a 17 λ Diameter Circular Groundplane, With and Without an Anti-Phased Surface Wave Device.

22

difficulty of achieving surface-wave amplitude control via resistive loading (see Figure 14), the different phase center geometry presented to the five interferometer elements, and the expensive construction involved.

III. COMPLEMENTARY SLOT-DIPOLE ANALYSIS

The results of the limited antenna technique investigation discussed in the preceeding section indicated that the most practical solution for the interferometer application was the complementary slot-dipole combination. Pattern analysis can be carried out by referring back to Figure 6 and inserting a complementary slot radiator in the surface of the groundplane at the point directly beneath the dipole location. Note that the phase center of the slot is thereby coincident with the phase center of the dipole plus its image, and that the combination forms a three-element vertical array. The total field intensities in the principal pattern planes may be written by inspection as a simple extension of equations (10) and (11),

$$\text{(E-plane)} \quad E_E \approx 1 + A_d \sin u \cos \phi \, e^{-j\alpha} \tag{15}$$

$$\text{(H-plane)} \quad E_H \approx \cos \phi + A_d \sin u \, e^{-j\alpha} \tag{16}$$

where $u = (2\pi h/\lambda) \cos \phi$

α = phase lag of dipole excitation relative to the slot.

A_d = amplitude of dipole excitation relative to the slot.

An examination of equations (15) and (16) reveals that A_d must have a value close to unity in order for the E-plane and H-plane patterns to have approximately equal maxima; i.e., there should be approximately equal power division between the slot and the dipole. Secondly, the phase lag angle, α, should be restricted to within ±50 degrees of 2π in order to obtain a satisfactory dip in the pattern at zenith. And third, the height, h, is restricted to the range,

$$0.5 < \left(\frac{h}{\lambda}\right) < 0.75$$

23
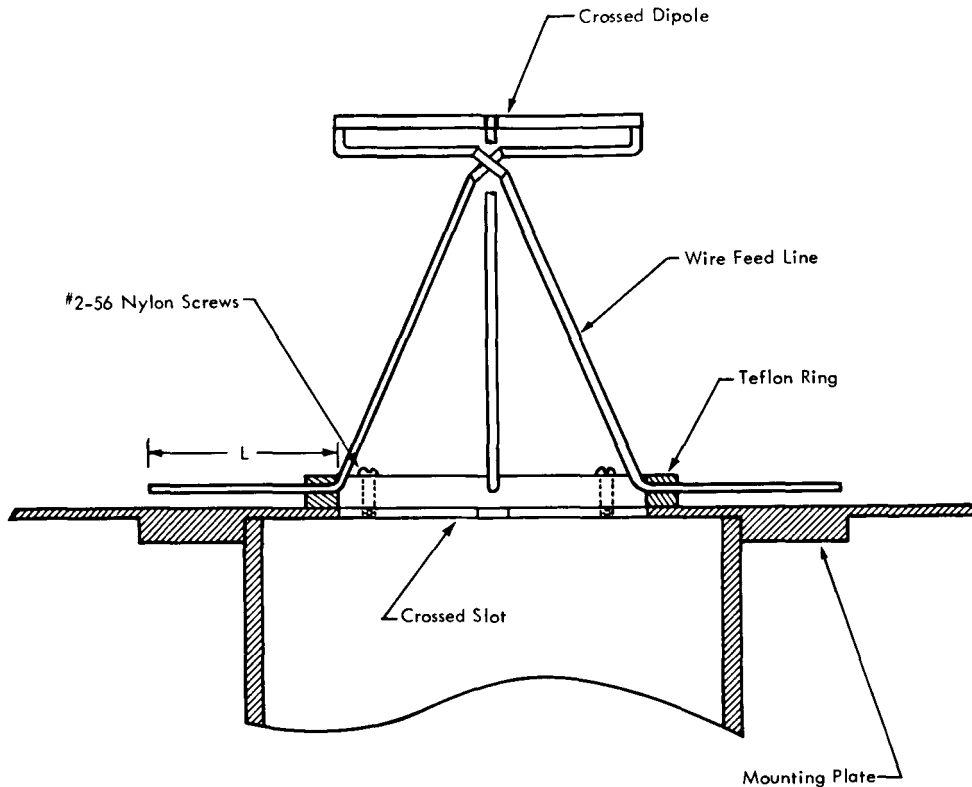
Figure 17—Complementary Crossed, Folded Dipole Mounted Over Crossed-Slots
With a Circular Polarization Waveguide Feed Input.

Thus, there exists a very reasonable range of pair values for h and α which will produce a satisfactory approximation to the desired cosecant pattern.

There are several different dipole designs and feeding arrangements that can be utilized for the complementary slot-dipole, but the particular one chosen for the interferometer application is shown in Figure 17. This design consists of a crossed, folded dipole mounted over a crossed-slot which is flush-mounted in the groundplane and fed from below with a circular polarization waveguide feed. The impedance of a slot radiator (14) is about 800 ohms, whereas the impedance of the folded dipole (15) is approximately 300 ohms, so that some sort of impedance transforming device is needed to increase the dipole impedance at the point where it appears in shunt across the slot. This impedance transformation is accomplished by the spread-leg two-wire transmission line section illustrated in Figure 17. The tapered, high-impedance section of balanced line serves to increase the dipole impedance so that the RF power divides rather evenly between the slot and the dipole as required by equations (15) and (16).

24

Fine-adjustment phasing of the dipole is accomplished via the length, L, of open wire line shown in Figure 17. This open wire plus its ground-plane image form a section of transmission line which is in series with the transformed impedance of the dipole, resulting in the series reactance,

$$Z = -jZ_0 \cot \frac{2\pi L}{\lambda} \,. \tag{17}$$

Thus, it is possible to vary the phase angle α somewhat, and experimental pattern measurements show that this adjustment is quite effective. Length, L, is generally close to $\lambda/4$ for best results.

Coarse phasing of the dipole is dependent upon the total transmission-line pathlength between the slot and the dipole itself, with most of the phase delay being due to the height, h, of the dipole above the slot. A 180° phase adjustment is available by crossing the balanced two-wire line at the point where it feeds the folded dipole. Note that this phase reversal is incorporated in the Figure 17 design.

Having discussed the physical arrangement of the antenna, it is of interest to substitute typical values for A_d, α, and h into equations (15) and (16) for calculation of the E-plane and H-plane patterns. A typical set of values would be the following:

$$A_d = 1$$

$$\alpha = \pm 37°$$

$$h = 0.58\lambda$$

The results of the calculations are plotted in Figure 18. The E-plane equation (15) was modified in the region $80° \leq \phi \leq 90°$ to include the edge diffraction drop-off of the slot as obtained from Figure 8. It will be noted that the two patterns follow one another fairly well except near the horizon ($\phi = 90°$), where the H-plane pattern rapidly drops away to zero while the E-plane remains relatively high.

Patterns measured on an X-band model of the complementary slot-dipole with h = 0.58λ are shown in Figure 19 for comparison. The agreement is considered to be reasonably good. The major differences are attributable to the effects of diffraction at the edges of the ground-plane, particularly for the E-plane pattern.

25
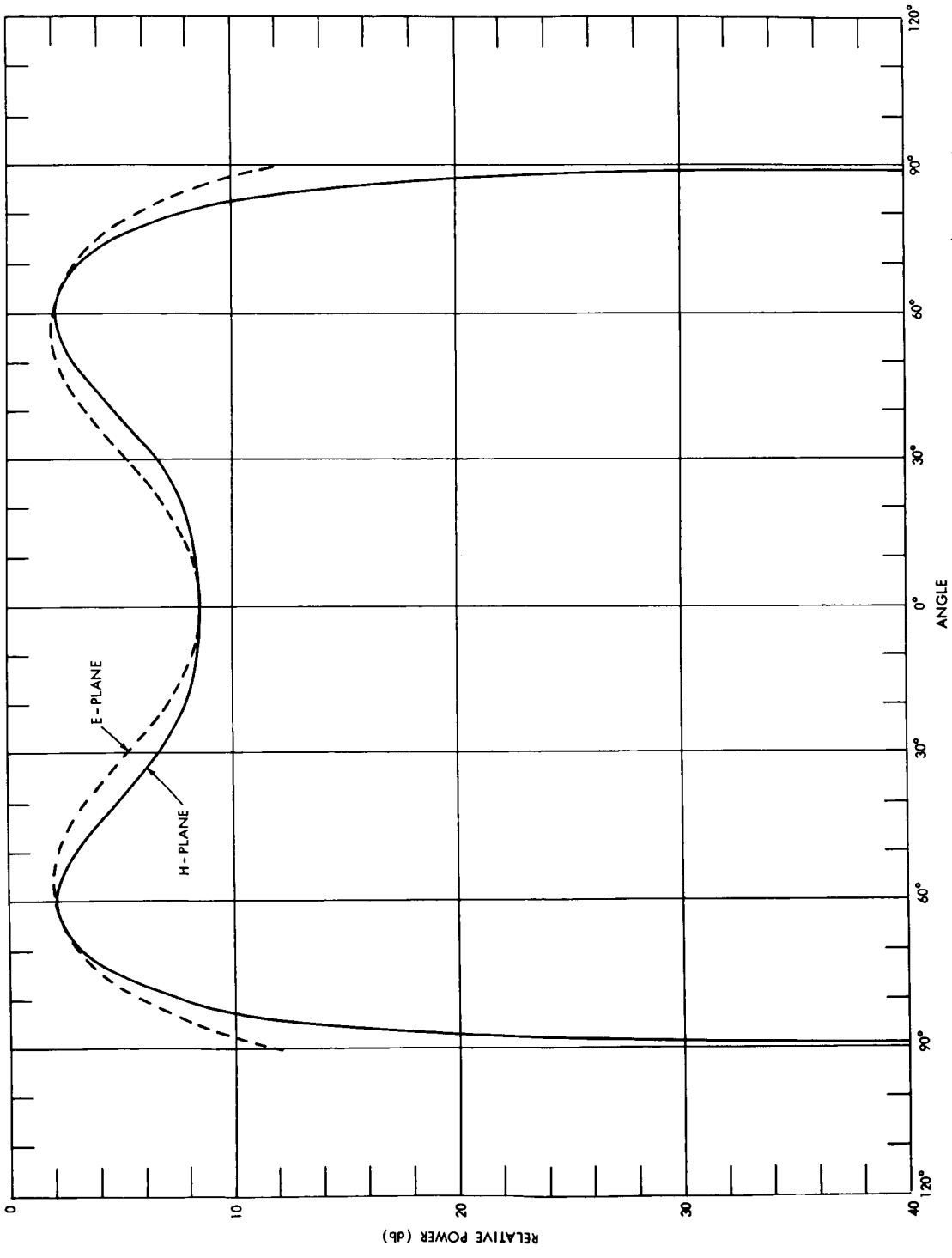
Figure 18—Principal Plane Power Patterns Calculated For Complementary Slot-Dipole Antenna Assuming h = 0.58 λ; α = ± 37°, and A_d = 1. E-plane Pattern Includes Diffraction Slope in the Region $80° \leq \phi \leq 90°$.
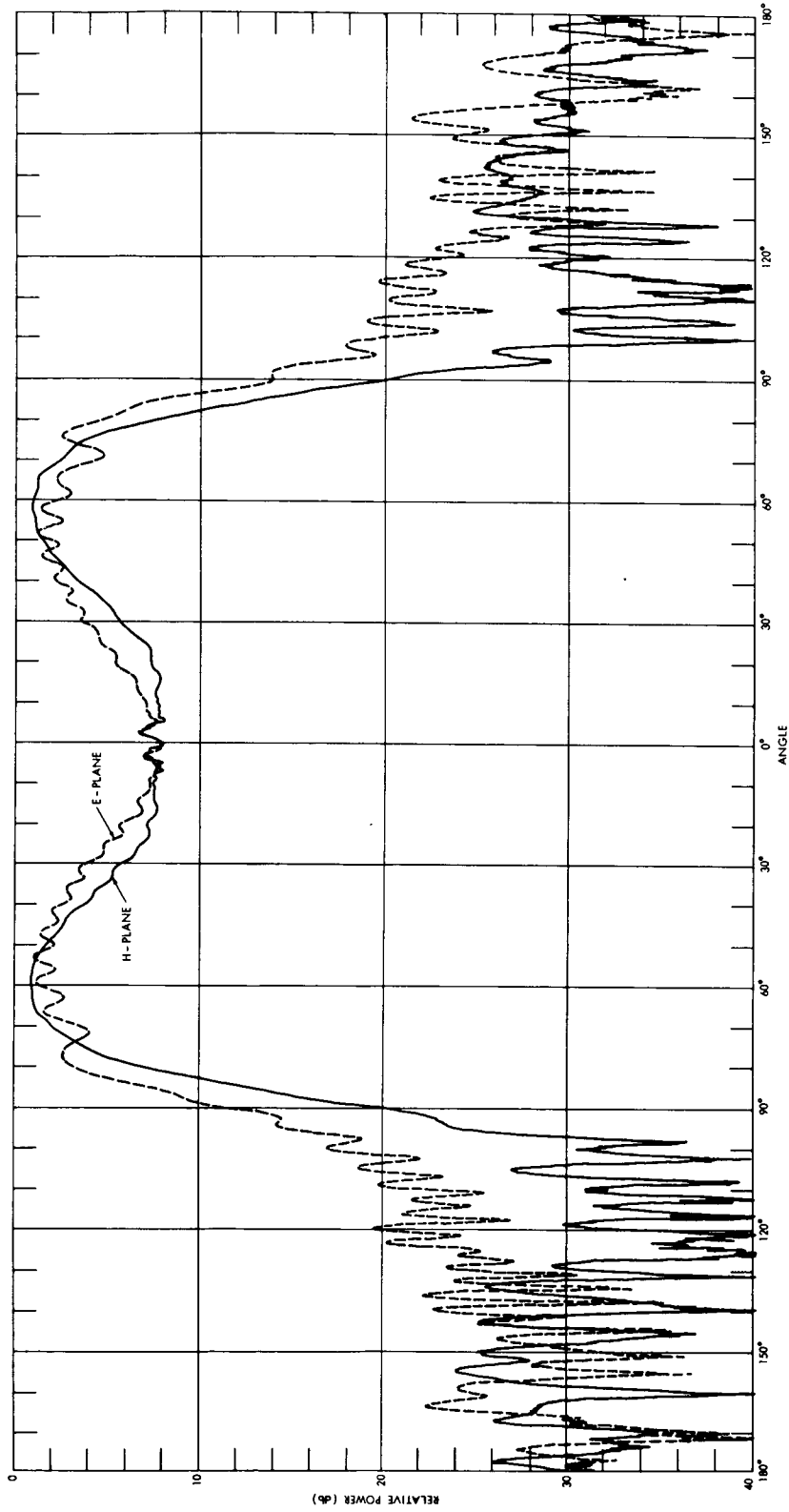
Figure 19—Principal Plane Patterns Measured on an X-Band Model of the Complementary Slot-Dipole Antenna With h = 0.58 λ; L = 0.24 λ; 9.15 GHz., 25 λ Square Groundplane; and Diagonal Orientation.

The relatively high illumination of the groundplane edge by the E-plane radiation of the slots causes a back-radiation level which may be too high for some antenna site locations. If site problems caused by large specular reflections should exist, the back-radiation level may be reduced by extending absorbing material beyond the ground-plane edges and/or extending absorber-loaded quarter-wave choke grooves beyond the groundplane edges. It also is very helpful to mount the groundplane as high as possible above the surrounding terrain and adjacent structures.

IV. FINAL DESIGN AND PERFORMANCE DATA

The complementary slot-dipole antenna was fabricated at S-band based upon the X-band scale model experimentation. The S-band antenna is shown in Figure 20. The crossed dipoles are supported by the orthogonal two wire transmission lines. The transmission lines are mounted on a teflon ring above the crossed slots. A circular wave-guide-to-coaxial transition feeds the slots from below the groundplane. The dimensions of the antenna components are given in Figures 21, 22, 23, and 24. The complete interferometer consisting of the five antennas mounted on a groundplane is shown in Figure 1. Each antenna is covered with a hemispherical fibreglass radome for weather protection. The radome dimensions are shown in Figure 25.
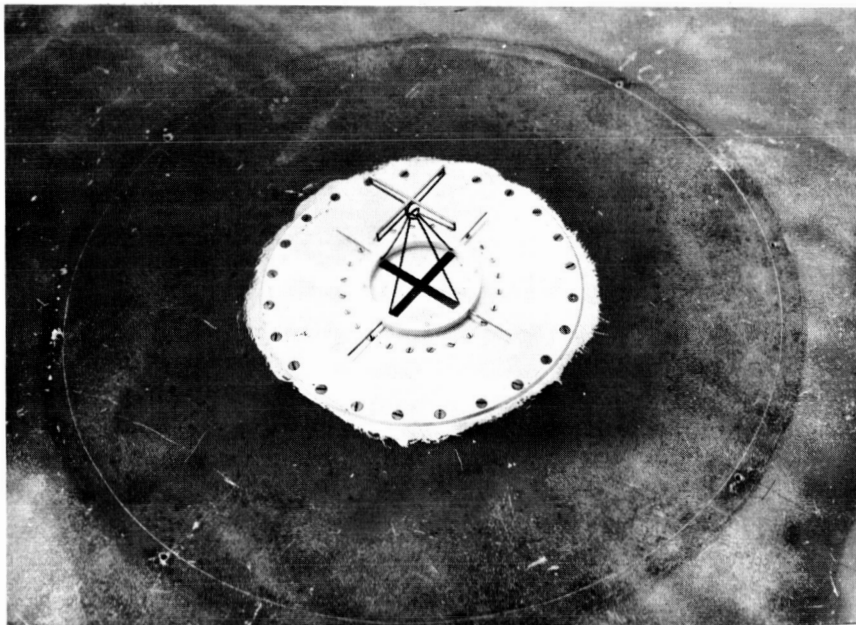
Figure 20—S-Band Complementary Slot-Dipole Mounted on Groundplane.
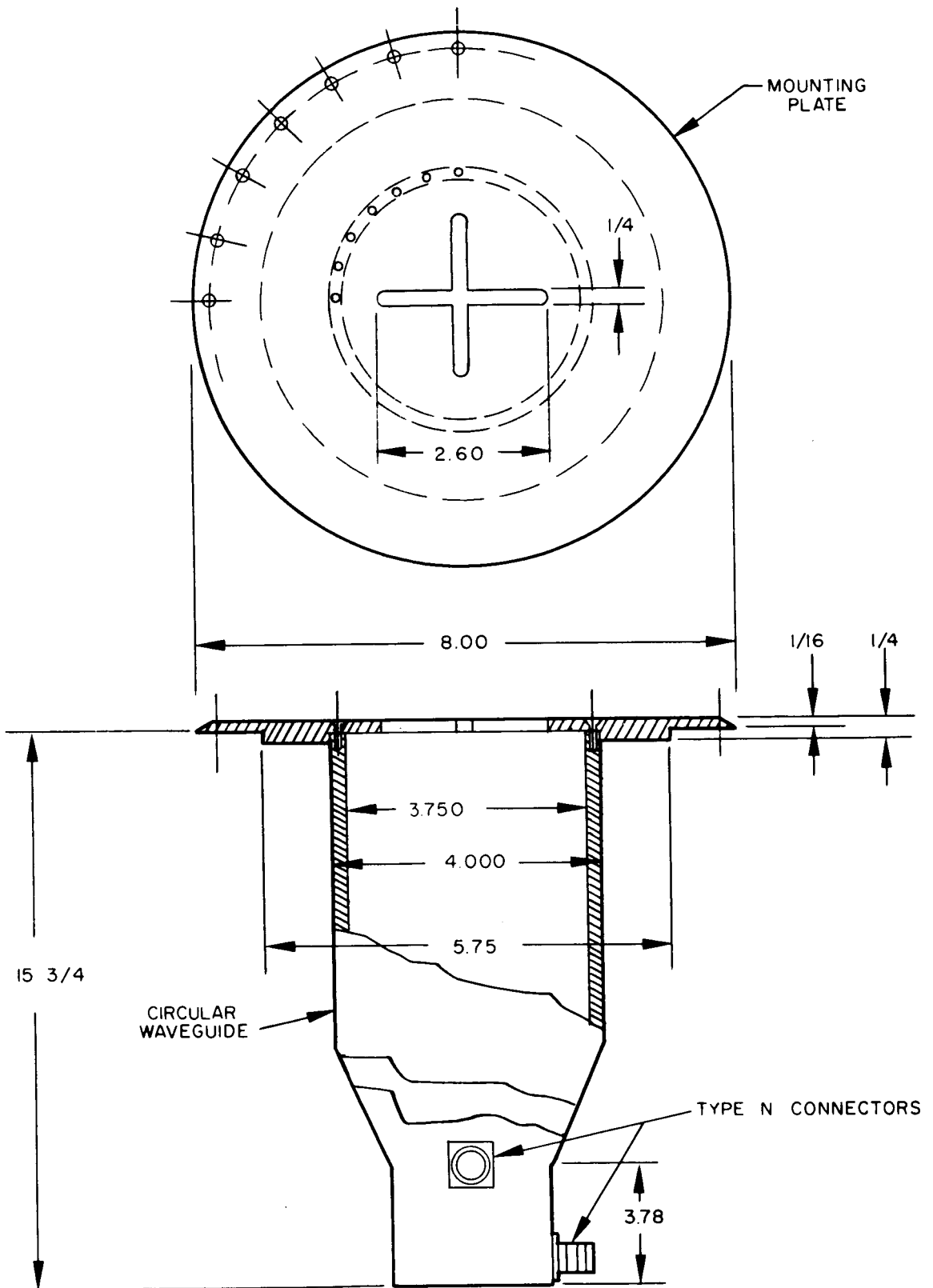
Figure 21–Crossed Slot and Waveguide Transition Feed

The figure contains the following labels and dimensions:

- MOUNTING PLATE
- 1/4
- 2.60
- 8.00
- 1/16
- 1/4
- 3.750
- 4.000
- 5.75
- 15 3/4
- CIRCULAR WAVEGUIDE
- TYPE N CONNECTORS
- 3.78
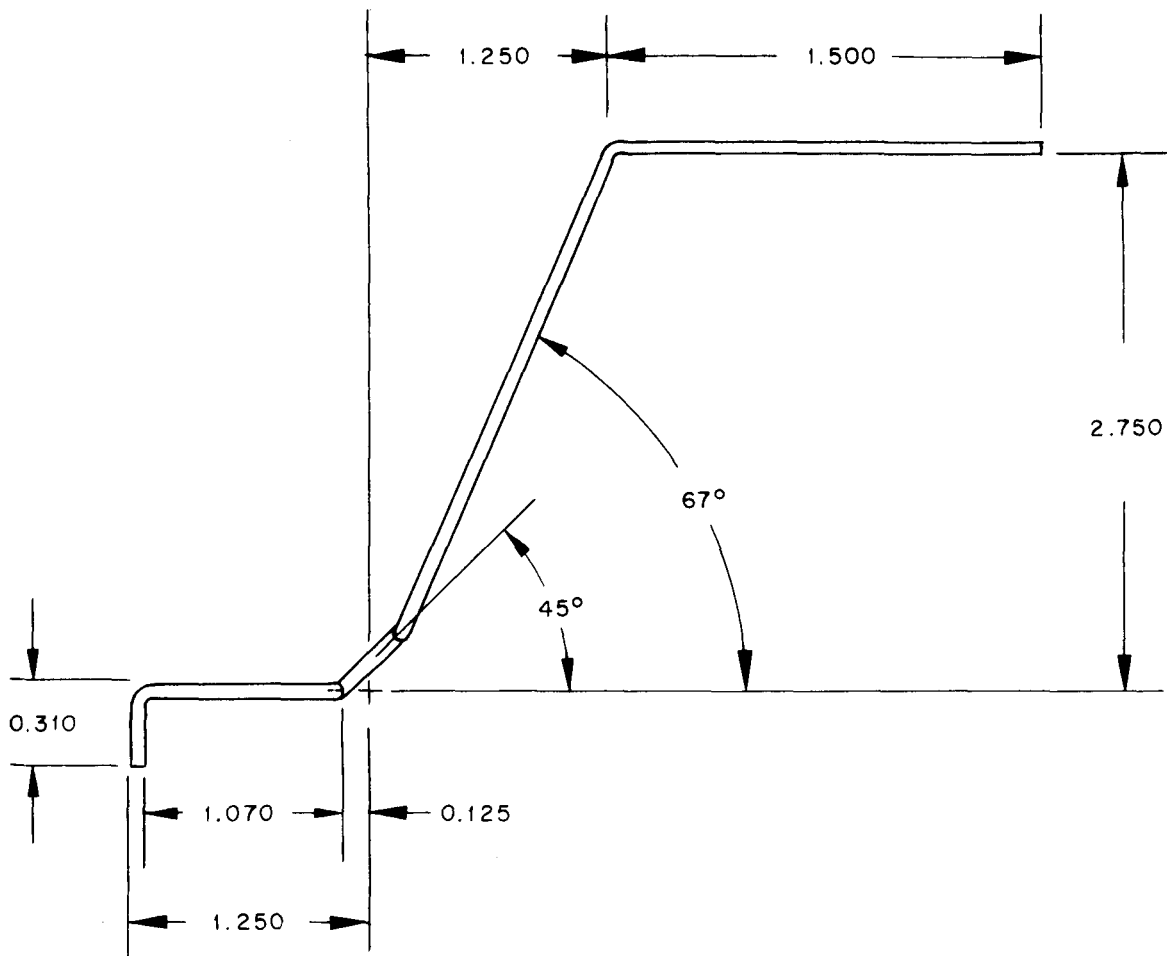
Figure 22—Wire Feed Line

The baseline lengths were established to a tolerance of .003 inches from the calculated values, and the groundplane containing the antennas is leveled to within 1/16 inch.

Typical radiation patterns for the S-band slot-dipole are shown in Figure 26 for the antenna mounted on a 18.5λ square groundplane. These S-band patterns are in good agreement with the X-band model patterns of Figure 19.

Impedance matching of the slot-dipole was adjusted by a 0.25 inch thick teflon cylinder positioned in the circular waveguide feed. The s.w.r. of the five antenna installed in the 37.5λ groundplane was less than 1.20 to 1 at 2287.5 MHz.
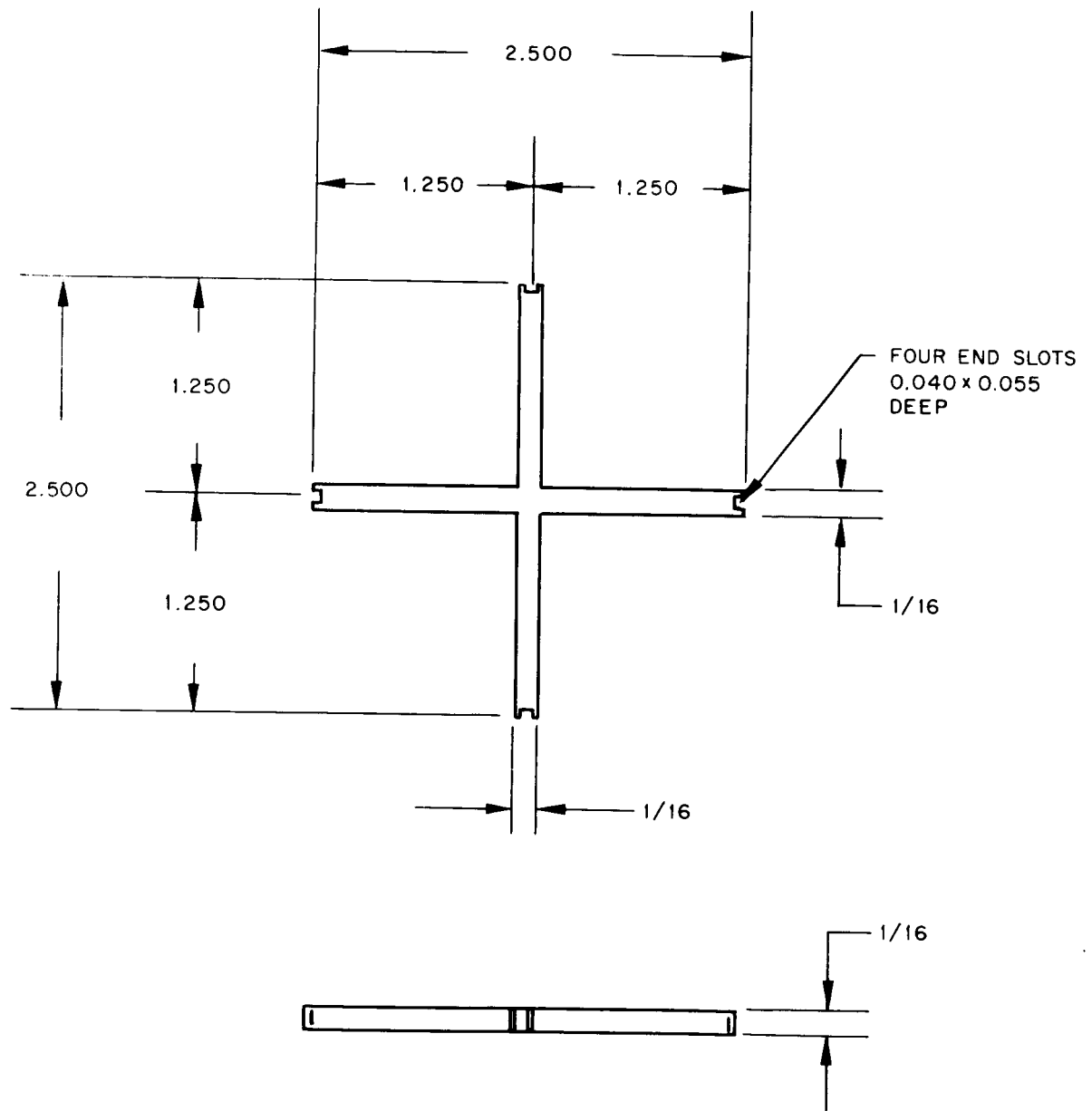
Figure 23—Crossed Dipole

2.500

3.000

0.250   0.155

ϕ

Figure 24–Teflon Ring

FIBREGLASS
0.025

8.5 R

0.060

17.5 d

18 d
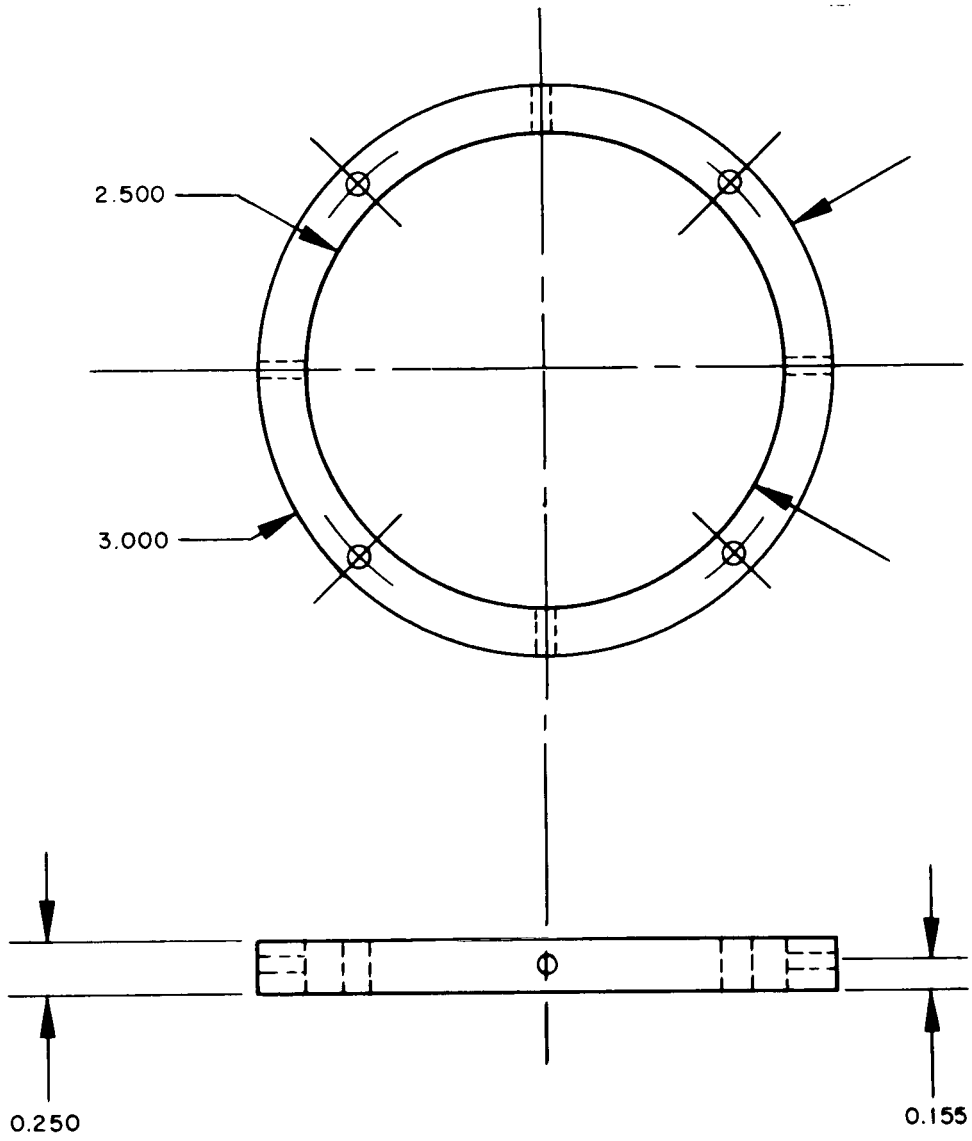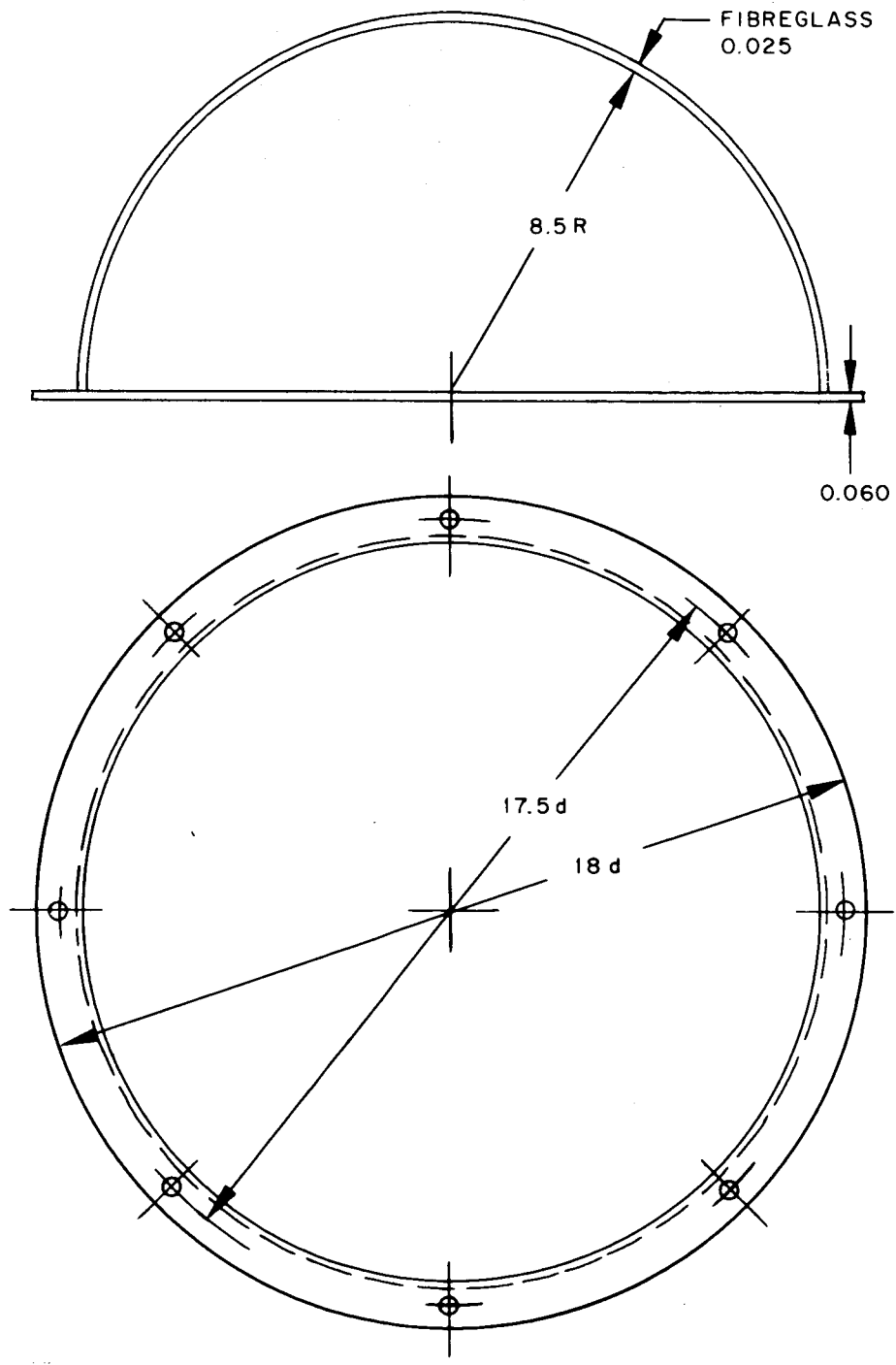
Figure 25-Hemispherical Radome
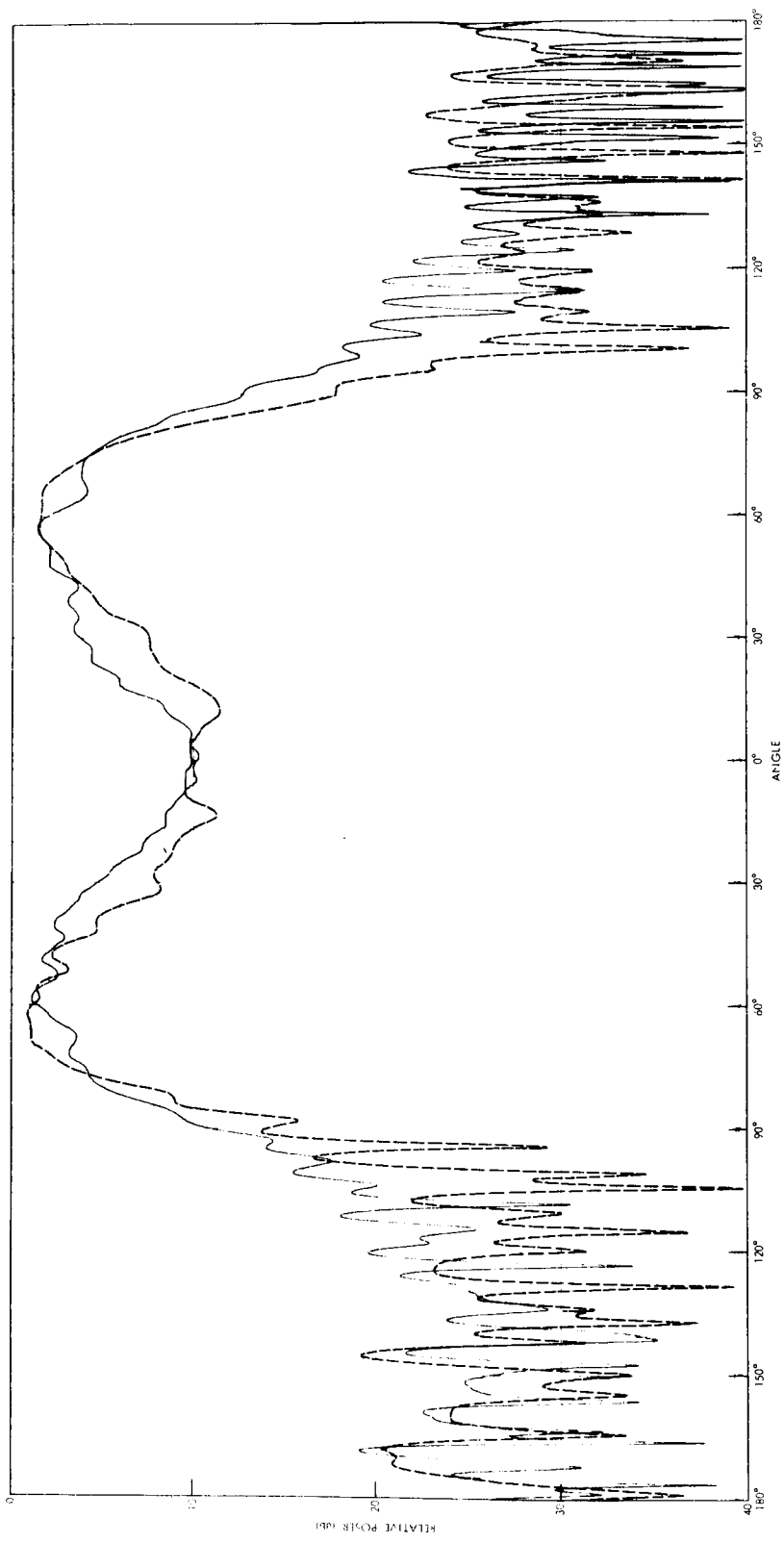
Figure 26—Radiation Patterns in E and H Plane of the S-Band Slot-Dipole on a 18.5 λ Square Groundplane.

34

V. ACKNOWLEDGEMENTS

REFERENCES

1. F. O. Vonbun, "Re-Entry Tracking For APOLLO," NASA X-513-64-85, March 6, 1964.

2. V. R. Simas, "A System For Re-Entry Tracking of the APOLLO Spacecraft," NASA X-523-63-56, April 2, 1963.

3. M. I. Skolnik, "Introduction to Radar Systems," McGraw Hill, 1962, pp. 59-60.

4. V. R. Simas, "Signal Level Performance of the Interferometer Re-Entry Tracker," X-523-65-199, May 10, 1965.

5. J. D. Kraus, "Antennas," McGraw Hill Book Company, Inc., New York, 1950. (Refer to Chapter 4)

6. E. C. Jordan, "Electromagnetic Waves and Radiating Systems," Prentice-Hall, Inc., New Jersey, 1950. (Refer to Chapter 12)

7. V. Galindo and K. Green, "A Near-Isotropic Circularly Polarized Antenna for Space Vehicles," IEEE Transactions on Antennas and Propagation, Vol. AP-13, pp. 872-877, November 1965.

8. See Reference 6, pp. 573-577.

9. P. M. Russo, R. C. Rudduck, and L. Peters, "A Method for Computing E-Plane Patterns of Horn Antennas," IEEE Transactions On Antennas And Propagation, Vol. AP-13, pp. 219-224, March 1965.

10. D. Schuster, E. T. Stelzried, and G. S. Levy, "The Determination of Noise Temperatures of Large Paraboloidal Antennas," IRE Transactions On Antennas and Propagation, Vol. AP-10, pp. 286-291, May 1962.

11. A. F. Kay, "The Scalar Feed," AFCRL Report No. 64-347, March 1964; Scientific Report No. 5 under Contract AF 19 (604)-8057, Project 4600, Task 460002; Astia Document 601609.

12. A. F. Kay, "Wide Angle Horn Feed Closely Spaced To Main Reflector," U. S. Patent No. 3,216, 018, Filed October 12, 1962.

13. Henry Jasik, "Antenna Engineering Handbook," McGraw Hill Book Company, Inc., New York, 1961. (Refer to Chapter 16)

14. See Reference 13, Chapter 8.

15. See Reference 13, Chapter 3.

APPENDIX I

The phase difference, ψ, between two identical antennas separated by a distance, d, is related to the space angle, θ, of the source, by the relationship

$$\psi = \frac{2\pi d}{\lambda} \cos \theta$$

as shown in figure 2. If

$$\theta = f(d, \lambda, \psi),$$

then

$$\cos \theta = \frac{\psi \lambda}{2\pi d}$$

and differentiating,

$$\sin \theta \ \delta\theta = \frac{\lambda}{2\pi d} \ \delta\psi + \frac{\psi}{2\pi d} \ \delta\lambda - \frac{\psi\lambda}{2\pi d^2} \ \delta d$$

$$\delta\theta = \frac{1}{2\pi \sin \theta} \left(\frac{\lambda}{d}\right) \left\{\delta\psi + \psi \frac{\delta\lambda}{\lambda} - \psi \frac{\delta d}{d}\right\}$$

Substituting the original phase expression for ψ

$$\delta\theta = \left\{\frac{1}{2\pi \sin \theta} \left(\frac{\lambda}{d}\right) \left[\delta\psi + \frac{2\pi d}{\lambda} \cos \theta \left(\frac{\delta\lambda}{\lambda} - \frac{\delta d}{d}\right)\right]\right\}$$

This expression relates the error in space angle, $\delta\theta$, due to errors in phase, $\delta\psi$, wavelength, $\delta\lambda$, and baseline length, δd.

The phase error, $\delta\psi$, due to an error in baseline length, δd, may be found by equating the expression in brackets equal to zero and assuming constant wavelength. Then

$$\delta\psi = \frac{2\pi}{\lambda}\,\delta d\,\cos\,\theta.$$